NATIONAL WATER RESEARCH INSTITUTE

INSTITUT NATIONAL de RECHERCHE sur les EAUX

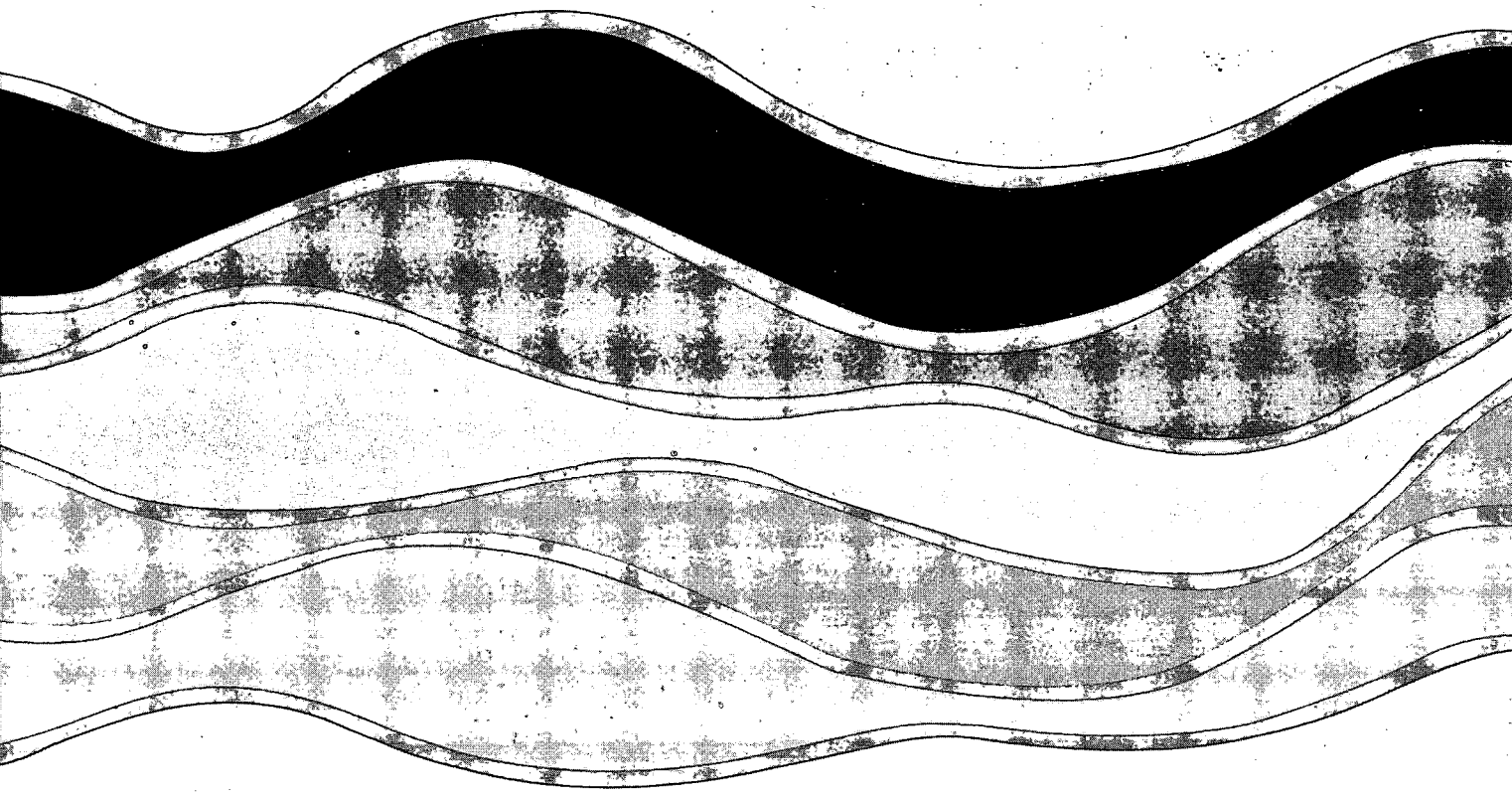

THE VELOCITY FIELD BENEATH WIND-WAVES

W.M. Drennan, K.K. Kahma and M.A. Donelan

NWRI Contribution No. 91-118

THE VELOCITY FIELD BENEATH WIND-WAVES

W.M. Drennan, K.K. Kahma[1] and M.A. Donelan

National Water Research Institute
Burlington, Ontario L7R 4A6

[1]Finnish Institute of Marine Research
P.O. Box 33, Helsinki, Finland

NWRI Contribution No. 91-118

MANAGEMENT PERSPECTIVE

The hydrodynamics of deep water wave breaking (whitecapping) is particularly relevant to the development of Canada's conventional offshore energy resources. New knowledge of it will be applied to engineering design, operational efficiency and safety, and environmental protection through improved estimation of wave-induced forces and improved understanding of mixing processes. This report, sponsored in part by the Panel on Energy Research and Development, presents results from the WAVES field experiment of 1985-1987.

PERSPECTIVE DE LA DIRECTION

L'hydrodynamique du déferlement des vagues en eau profonde (moutons) est particulièrement pertinente dans la contexte de la mise en valeur des ressources de pétrole et de gaz situées au large des côtes canadiens. Une meilleure capacité de prédire les forces causées par les vagues et des connaissances accrues des processus de mélange seront un apport important dans la conception des structures ainsi que pour leur éfficacité, leur sécurité et la protection de l'environnement. Ce rapport, partiellement financé par le Groupe interministériel de recherche et développemente énergétiques, présente les résultats de la campagne de mesures WAVES pendant la période 1985 à 1987.

ABSTRACT

An extensive set of measurements taken from a fixed tower is used to study the velocity field under wind waves. Velocity measurements, made with miniature drag spheres, are compared with linear theory estimates of the orbital velocities obtained from measured surface elevation. Results are presented in the context of how well linear theory is able to predict wave-induced forces on cylindrical structural members.

The velocity measurements are also used to study turbulent energy dissipation in the near surface region. Analysis based on spectral densities in the inertial subrange yields dissipation rate estimates several orders of magnitude larger than would be expected if turbulence followed classical wall layer scaling.

RÉSUMÉ

Une vaste base de données, recueillie à partir d'une plateforme permanente, est utilisée pour l'étude du champs de vitesse de vagues produites par le vent. Les vitesses sont évaluées à partir de sphères miniatures qui mesurent la trainée hydraulique. Ces données sont comparées aux vitesses orbitales obtenues par application de la théorie linéaire à partir de mesures de profil de surface. Les resultats sont rapportés de façon à mettre en evidence la précision de cette méthode lorsqu'utilisée pour la prédiction des forces sur des cylindres submergées.

Les mesures des vitesse ont aussi servi à l'étude de la dissipation turbulente de l'énergie près de la surface. A partir d'une analyse des densités spectral dans la région de la sous-rang inertiel de la turbulence isotropique, des valeurs de taux de dissipation obtenues dépassent de plusieurs ordre de grandeur celles prévues par la théorie classique d'écoulement près d'un mur rigide.

1. INTRODUCTION

The design of cost-effective offshore structures is highly dependent on an accurate estimation of wave forces which, in turn, depend on the wave orbital velocities, accelerations and pressures. Very few measurements have been made of actual velocities beneath natural wind-generated waves and the design engineer generally relies on linear wave theory to derive appropriate design forces from a suitable climatology of wave (surface elevation) information. Recent results, however, show that the predicted forces can differ from observed ones by as much as 50 to 100% (Ramberg and Niedzwecki, 1979). A large part of this uncertainty is due to inaccuracies in the model by which flow velocities (and thence forces which are related to the square of velocity) are calculated. Although laboratory studies (e.g. Vis, 1980) have generally indicated good agreement between measured and predicted velocities, conditions in the field can differ dramatically from those in the laboratory. In particular, the presence of variable currents and the high local accelerations associated with wave breaking (see Melville and Rapp, 1985) can have important consequences on local velocities and wave forces.

Typically, the forces are predicted using Morison's equation,

$$F_u(t) = C_D \rho r u(t) |u(t)| + C_M \rho \pi r^2 \dot{u}(t) \tag{1}$$

(Morison *et al.*, 1950), which estimates the incremental horizontal force per unit length exerted by a moving fluid on a fixed vertical cylinder. Here, ρ is the fluid density, r is the radius of the cylinder, C_D and C_M are drag and inertial coefficients and $u(t)$ and $\dot{u}(t)$ are horizontal fluid velocity and acceleration. C_D and C_M are functions of the Reynolds number $R_e = 2|u|r/\nu$, the relative surface roughness $(k_d/2r)$ and the Keulegan-Carpenter number $N_{kc} = AT/2r$, where ν is the fluid kinematic viscosity, k_d is the average roughness diameter, A is the velocity amplitude of the oscillatory part of the flow, and T is it's period.

Morison's equation ignores wave drag, which occurs if the cylinder is at or near density interfaces, and skin drag. Nevertheless, for most engineering applications the form drag and inertial resistance modelled by Morison's equation are the dominant forces. Laboratory measurements on the in-line (with horizontal velocity) force on vertical cylinders seem to agree well with that deduced from Morison's equation (Bearman et al., 1985).

The behaviour of the drag and inertial coefficients with Reynolds and Keulegan-Carpenter numbers has been the subject of many investigations (see Sarpkaya and Isaacson, 1981 for a summary), most of which have been carried out in laboratories under idealized conditions of uni-directional, planar oscillatory or circular oscillatory flows. Strong Reynolds number and Keulegan-Carpenter number dependencies on the drag and inertial coefficients imply that the standard practice of using constant values for these coefficients for force calculations over the entire length of vertical cylinders is fraught with error (Ramberg and Niedzwecki, 1979). An additional source of error arises in the calculation of orbital velocities from observed surface elevations using theoretical models. For irregular seas, these models are based on linear theory and one or two ad hoc assumptions. However, a new model by Donelan, Anctil and Doering (1991) has a firmer theoretical foundation and has shown favourable comparisons against laboratory data.

Over the past few decades, several papers have appeared comparing measured field velocities with those predicted by linear theory. Both Guza and Thornton (1980) and Thornton and Krapohl (1974) investigating, respectively, shoaling waves and swell, report good agreement between observed and measured flow velocities – typically to within 10% . Simpson (1969) with measurements in 6 metres of water off the end of a pier finds similar results, with discrepancies of up to 15% in velocity. There are, however, important differences between two recent works dealing with active wind sea

conditions. While both Battjes and van Heteren (1984) and Cavaleri, Ewing and Smith (1977) report fairly good agreement (to within 20%) between measured and predicted velocity magnitudes, Cavaleri, Ewing and Smith report observations indicating that the phase between horizontal and vertical velocity components can be substantially different from that predicted. In particular, under active wind-sea conditions these discrepancies were typically around 30°. Similar results have been observed by Shonting (1970). This phase difference which cannot be explained by linear theory would have, if confirmed, important implications for momentum transport rates in the water column: typically, it implies a momentum transfer many times larger than the momentum input from the wind at the surface !

Although most of the above comparisons are carried out between measured and predicted r.m.s. velocities, from the point of view of structural design it is the peak velocities which are most significant. As the steepest waves tend to be the most nonlinear, the question must be asked as to how well linear theory predicts the peak velocities. Thus, the matter of predicting velocities and wave forces in an active wind-sea is far from settled and it was partly to resolve these issues that the WAVES (Water-Air Vertical Exchange Studies) experiments were carried out (Donelan and Kahma, 1987).

Finally, the same features which influence the accuracy of calculated wave forces – flow nonlinearities and wave breaking, among others – have important consequences for processes occurring in the near-surface layer of the ocean, in particular mixing and the dispersal of buoyant pollutants. One issue, which we address here, relates to the dissipation rate of turbulent energy in the near-surface region. According to Soloviev *et al.* (1988) most field results from the past two decades show dissipation rates to be consistent with turbulent energy derived from current shear alone – with no additional energy input due to wave breaking. These data, however, are generally taken

over short time intervals , in relatively calm conditions and at moderate depths, all of which could minimize the effects of breaking, which is an intermittant phenomenon. In fact, the one data set which contradicts these conclusions, that of Kitaigorodskii *et al.* (1983), was collected in strongly forced conditions near the surface and over longer time intervals. The velocity measurements of the WAVES experiments, taken over a wide range of conditions, will be employed to address this issue.

2. EXPERIMENT

A fixed tower provides the ideal platform for measurements of sub-surface velocities and that of the National Water Research Institute in Lake Ontario is particularly well suited to this purpose. Having been designed expressly for wave measurements, the tower is free of cross-bracing in the vicinity of the water surface (see Figure 1). The tower is situated 1.1 kilometres offshore in 12.5 metres of water, as indicated in Figure 2. The tower is supplied with power via underwater cables and 48 channels of data, sampled at 20 Hz by computer, are transmitted by cable to shore. Further details of the research site are given in Donelan *et al.* (1985).

The instruments used for measuring both vertical and horizontal components of velocity were "drag spheres", in which the fluid force on a sphere yields a measure of the velocity components (Donelan and Motycka, 1978). The original set-up used in 1985 consisted of three drag spheres mounted on a rotatable mast at depths of about 1.2 m, 2 m and 4 m. In 1987 there were two drag spheres at depths of about 60 cm and 170 cm. The mast could be rotated by control from the shore station so that the axes of the drag spheres were aligned normal to the mean wave direction. The instruments thus yielded vertical and horizontal (down-wave) velocity components. The size of the drag spheres (4 mm diameter) was such that they responded essentially to drag and not to inertial effects in the range of wave heights and periods expected (Donelan and Motycka, 1978).

Since the drag response is nonlinear (almost perfectly a square law in the Reynold's number range used), the instruments were zeroed mechanically before and after each measurement run by means of pneumatically activated sleeves that shielded the drag spheres from the ambient flows. The drag spheres were carefully calibrated both before and after field exposure. Calibration was accomplished by towing the instruments in the 120 m towing tank of the National Water Research Institute.

In addition to the drag sphere measurements, ten wave staffs were deployed at various locations around the tower to provide wave height information. Of particular interest to this report is a wave staff located near the mast rotator, about 50 cm from the drag spheres. We also report mean wave directional properties obtained from an array of six wave staffs (a pentagon of 25 cm radius, with an additional staff in the center). More detailed wave directional information may be found in Tsanis and Donelan (1989). An anemometer-bivane situated on a mast about 12 m above the water surface yielded measurements of wind speed U_{12} and direction (θ_w). Measurements of relative humidity and air and water temperatures were also recorded.

3. ANALYSIS

The experimental phase of the WAVES experiment took place during the fall seasons of 1985, 1986 and 1987. Altogether some 300 data runs of sixty to ninety minutes duration were made. During 1987, an additional forty or so 'monitor' runs of ten minute averages were recorded so as to fill in the 'gaps' between data runs. The subsequent analysis has concentrated on the data of 1985 (when three drag spheres were available) and 1987 (when there is also data from a string of 12 acoustic current metres and a laser-doppler velocimeter). Processing of the drag sphere and associated wave staff data has consisted of applying spectral analysis using fast Fourier transforms (FFTs) based on blocks of 8192 points (6.83 minutes). This choice of block length

permitted interpretation of some of the lower frequency information (to under 0.01 Hz.), while giving enough independent blocks for reliable statistical estimation. To reduce contamination of the low spectral densities through window leakage from the peak, a 4-term Blackman-Harris taper (Harris, 1978) was applied to the individual blocks. Four adjacent spectral estimates are averaged so that each plotted point has 64 degrees of freedom (for the 90 minute runs) corresponding to 95% confidence levels of 1.28 and 0.72.

The implementation of linear theory was based on wave height measurements taken at a wave staff offset 22.5 cm downwave and 45 cm crosswave from the drag spheres. The water depth d and distance of the drag sphere below the surface z were based on the mean water level during the run. The wave height signals were Fourier transformed as described above so as to calculate the Fourier coefficients. The wave number k associated with each frequency f was then calculated from linear theory, along with the quantities

$$T_{\eta u} = 2\pi f \frac{\cosh(k(d-z))}{\sinh(kd)} e^{i\phi_{\eta u}} \quad \text{and} \quad T_{\eta w} = 2\pi i f \frac{\cosh(k(d-z))}{\cosh(kd)} e^{i\phi_{\eta u}}, \qquad (2)$$

which represent the transfer functions between the surface elevation η and velocities u and w, respectively. The quantity $\phi_{\eta u}$ corrects for the phase shift (with frequency) due to the downwave spatial offset between the wave staff and drag spheres, along with that induced by sampling and electronic filtration. Finally, the linear theory velocity estimates u_l and w_l were determined by inverse Fourier transform. We note here that unidirectional long-crested waves were assumed with the result that u_l and w_l are 90° out of phase.

For determining the directional spectra, data collected from each of the six wave staffs of the array were averaged down to 4 Hz, and cross spectra were calculated based on blocks of 1024 points. A maximum likelihood method (MLM) based on Jefferys (1986) with 10 degree directional spacing was employed. Only selected results

from the directional analysis will be presented here; more detailed results are available in Tsanis and Donelan (1989).

4. RESULTS

4.1 Data summary

In Table 1, we present a summary of the meteorological conditions present during each WAVES experimental run. It has been found convenient to classify the runs by weather event. The prevailing winds in the area are from the southwest, and for these cases, the fetch at the tower is of the order of one to two kilometres. Storms tracking south of Lake Ontario often result in winds from the east, and for these cases the fetch at the tower is of the order of 200 to 300 kilometres. Consequently, a classification of the runs by wind direction is essentially a classification by wave development: waves from the west are fetch limited, with a corresponding low wave age, while those from the east tend to be older or greater developed.

After careful initial analysis, it became evident that the sensitivity of the drag spheres had changed during the two months of the 1987 experiment. While the calibrations carried out before and after the 1985 three week measuring period differed by only 3% to 9% , the calibrations of February 1988 were up to 20% higher than those of October 1987. A close inspection of the instruments revealed that during the much longer period of operation at higher water tempertures than during the previous years, biological material had grown on the sphere and on the supporting rod. Comparisons with linear theory suggest that the instrument was actually more sensitive towards the end of the 1987 experiment than it was during the post-experiment calibrations after two months of drying. In virtually all of the 1985 runs, linear theory appears to fit the data well whereas in 1987 the deviation becomes larger and larger with time. This

deviation is independent of frequency, consistent with the idea that it results from a change in the sensitivity.

The comparison with linear theory is therefore based on the 1985 data set alone. Linear theory will then be used as a calibration for the 1987 data. In Table 2, we summarize results for some fifteen runs for which a linear analysis was carried out. We have selected four runs for detailed presentation : 85105, 85111, 85145 and 85159. This subset was selected so as to represent a good cross-section of the conditions encountered: 85111 represents an overdeveloped sea ($U_{12}/c_p = 0.1$) with swell propagating eastward along the major axis of Lake Ontario; 85105 ($U_{12}/c_p = 0.9$), near fully developed waves from the east; 85145 ($U_{12}/c_p = 1.3$), an underdeveloped east wind case; 85159 ($U_{12}/c_p = 4.2$), with very underdeveloped (strongly forced) waves from the west. The strongly forced, fetch-limited waves of 85159 are akin to the steep duration-limited waves associated with the outbreak of a storm. In Figures 3-4, we show wave height and directional spectra for each of the four cases. Note that above the peak, the wave height spectra conform to a f^{-4} power law (Donelan *et al.* 1985). The three east wind cases show waves with frequencies near the spectral peak to be arriving from approximately 70°, which is the principal axis of Lake Ontario. Although the waves in 85159 are predominantly from the west (240°), there is also evidence of 6 second swell from the east.

4.2 Wave velocities

In Figures 5-6, we present spectra of the vertical velocity components as measured by the drag sphere, compared with those calculated according to linear theory; sections of the time series are also plotted (Figure 7). Note that agreement with linear theory is very good around the peak of the wave spectrum. Away from the peak (and several decades lower in spectral density) the deviations are caused by turbulence

generated by wind-driven sheared current and by wave breaking (Kitaigorodskii *et al.*, 1983). Note that the high frequency regions of the spectra (85105, 85111 and 85159) display slopes of -5/3, corresponding to the inertial subrange of isotropic turbulence – see Section 4.4. For purposes of calculating wave-induced forces on structures, these differences are less important than those occurring around the peak at substantially higher energy levels.

The tenth column of Table 2, which shows the ratio of the variances (i.e. the integrated velocity spectra) of w and w_l (G_w), provides a measure of how well the velocities are predicted by linear theory. Typically, G_w falls between 0.88 and 1.15, which corresponds to measured velocities within 7% of linear theory predictions. Note that, according to Figure 8, the larger ratio value for run 85119 is due to an underestimation of the swell component which, in this run, is comparatively large; again, the wind sea is well predicted by linear theory. Exceptions to this are runs 85104 (386 cm depth), 85135 (390 cm), 85140 (390 cm), 85159 (401 cm) and 85160 (170 cm), where the measurements are taken at relatively large depths with low significant wave height. For these cases, the ratio of variances G_w reaches as high as two. This is a result of very low wave energy at the depths of measurement: the drag sphere is out of its operating range. Consequently, the measurements in these cases are spurious. Omitting these obvious outliers, the mean and standard deviation of G_w are 1.02 and 0.11 respectively.

In the case of horizontal velocity linear theory again is seen to perform well (Fig. 9), although there appear to be deviations at frequencies about twice that of the peak, where linear theory is seen to overpredict the velocity. This phenomenon was previously observed by Forristall *et al.* (1978), who attributed it to flow nonlinearities. As pointed out by Battjes and van Heteren (1984) however, nonlinearities would tend to have the opposite effect. We attribute the overprediction to the increasing directional

spread of the wind sea above the peak (see below): linear theory estimates are based on unidirectional waves, and so ignore the effects of spreading. Note that in several cases (e.g. 85116) the horizontal velocities appear to be very poorly predicted by linear theory. For run 85116 $G_u = 0.25$, whereas $G_w = 1.07$. As a rule, efforts were made to ensure that the drag spheres were aligned normal to the wave direction, so that the measured horizontal velocity would correspond to that of the principal wave direction. For some runs, however, this was not achieved, resulting in the low G_u ratios observed.

As noted above, the directional spread of the wind sea is not taken into account in linear theory. This can be rectified by correcting the wave height spectra $S_{\eta\eta}$ following Donelan *et al.* (1985):

$$F(f,\theta) = \frac{1}{2} S_{\eta\eta}(f) \beta \, \mathrm{sech}^2 \beta \{\theta - \bar{\theta}(f)\} \tag{3}$$

where θ is the wave direction, $\bar{\theta}$ the mean wave direction and

$$\beta = 2.61(f/f_p)^{+1.3}; \qquad 0.56 < f/f_p < 0.95,$$

$$\beta = 2.28(f/f_p)^{-1.3}; \qquad 0.95 < f/f_p < 1.6,$$

$$\beta = 1.24; \qquad \text{otherwise},$$

where f_p refers to the peak frequency. To be consistent with linear theory, θ was taken to be the mean wave direction at the wave peak, $\bar{\theta}_p$. These corrected wave height spectra were then used to generate the corrected linear horizontal velocity spectra which are plotted using dotted curves in Figures 9 a) and d). Note that directional effects are seen to account for the overprediction of horizontal velocities by linear theory at frequencies above twice the peak.

In Table 2 (last column) we present the phase angle ϕ_{uw} between the horizontal and vertical velocity components as measured by the drag sphere. ϕ_{uw} is calculated from the cospectrum of the two time series and the single value reported is that found

by averaging phase angle values for frequencies around the peak, where the coherence between the two signals was greater than 0.95. For the four selected runs, the phase angle (along with 95% confidence limits calculated according to Bendat and Piersol, 1971) and coherence γ^2 are plotted, for frequencies around the peak, in Figures 10-11.

Although linear theory predicts a phase difference between u and w of exactly 90°, experimental results have not always supported this. In particular, Cavaleri *et al.* (1977, 1987) have reported consistent deviations from linear theory of as high as 30°, with current meter measurements taken in active wind sea conditions from a tower in the Adriatic Sea; measurements taken in swell show the expected phase lag of close to 90°. These results, if correct, would have important implications in the momentum balance, implying a surface flux considerably greater than that derived from wind input at the surface. Our results, taken over a wide range of meteorological conditions do not, however, corroborate these findings. On the contrary, our results support those of Battjes and van Heteren (1984), among others, in finding ϕ_{uw} to be consistent with linear theory predictions. It should be noted that reflected waves from nearby structures or topography can have a stong effect on the measured phase angle.

The paragraphs above indicate that linear theory is generally adequate for estimating the velocity field in a spectral sense. The question remains as to how well linear theory predicts the extreme waves of any event. In order to determine this, joint frequency distributions of u and u_l and of w and w_l were calculated for each of the runs. The corresponding plots for the four selected runs appear in Figure 12. Note that we have normalized u and u_l by $(\overline{u^2})^{1/2}$ and w and w_l by $(\overline{w^2})^{1/2}$. Also the mean flow (i.e. any current) has been subtracted from the measured velocities and all signals detrended. In the plots, curves of high aspect ratio, centred around the 45° line indicate that linear theory predicts the velocities on a wave by wave basis very well. In general, our data is seen to support this hypothesis although the contours for run 85159 display

significantly lower aspect ratios. Recall that this is a west wind case which implies short crested, high frequency waves. In such conditions, the 50 cm horizontal separation between the drag spheres and wave staff (measuring the wave heights employed in linear theory) will induce an error visible in wave-by-wave comparisons in that the two instruments will not always see the same wave. This is evident both in the time series plots (Fig. 7d) and in the broadening of the contours in the joint frequency distribution plots.

4.3 Wave forces

As pointed out in Section 1, wave forces on a vertical cylinder are typically estimated using Morison's equation (1), which requires knowledge of the flow field. This knowledge is often derived from wave height measurements by means of linear (or some other) theory as described above in Section 3. In this section, we compare the force estimates derived from linear theory to those based on drag sphere measurements. In particular, we compare the quantities $u|u|$ and $\dot{u}$. In Figure 13-14 examples of time series of $u|u|$ and $\dot{u}$ for the four selected runs are given; linear theory estimates are also shown. The time series segments chosen are coincident with those of Figure 7. We note here that during these runs, the drag spheres were aligned such that the measured horizontal velocity is down-wave and therefore comparable to linear theory velocities. Furthermore, directional spreading of the wind waves was taken into account following Donelan *et al.* (1985) - see above. The wave-by-wave comparisons of the drag force (Figure 13) show some discrepancies at both larger crests and troughs, but do not indicate any consistent over- or under-prediction.

Figure 15 illustrates the joint frequency distributions of the measured and predicted drag force, $u|u|$ and $u_l|u_l|$ for the four runs. It is evident that the distributions generally follow the 45° line, indicating good agreement between measured and pre-

dicted values, but that linear theory has a tendency to overpredict the larger forces under crests and to underpredict the larger forces under troughs, note the curvature in the contours, especially that of Figure 15a) or c). While similar curvature in a joint probability distribution may result from nonzero mean current, this is not the source of the curvature in Figure 15, because the mean has been subtracted from the velocities to avoid these distortions in the comparison. The deviation is likely related to the use of linear wave theory to model a finite amplitude wave field. This issue is addressed in Donelan *et al.* (1991).

A comparison (Figure 14) of the measured and predicted inertial forces, $\dot{u}$ and $\dot{u}_l$, shows clearly the effects of the high frequency turbulence on the measured velocity signal. While the force predicted by linear theory is smoothly varying with time, the measured force is seen to exhibit significant local accelerations due to the passage of turbulent eddies past the drag sphere. Consequently, the measured local forces are as high as twice those predicted by linear theory! We do note, however, that the linear term $\dot{u}_l$ does predict the measured force very well on a larger scale – that is, ignoring the turbulent local accelerations. The typical scale of these high local accelerations in our data is of order 10 cm and they therefore become significant for short bars which have a diameter about 5 cm. It appears that in general the Keulegan-Carpenter number for bars for which these local accelerations contribute significantly to the inertial forces can be approximated by $N_{kc} = 2f_c/f_p$, where f_p is the peak frequency and f_c the highest frequency of the turbulence which contributes significantly to the local accelerations.

It is thus seen that there are discrepancies between linear theory and measurements for both the drag and (especially) inertial forces. However, it is important to note that these force terms are implemented in Morison's equation with empirically calibrated coefficients. That is, the drag and inertial coefficients C_D and C_M are typically found through laboratory experiments in which a cylinder is subjected to a series

of waves (see Sarpkaya and Isaacson, 1981). The forces on the cylinder are typically measured with strain gauges, with the flow velocities being determined from the measured surface elevation *using linear theory*. Consequently, the differences between linear theory and measured forces, as noted above, are to a large degree taken into account through the empirical determination of the force coefficients for the conditions of the laboratory tests. However, as we have seen, the degree of deviation of the measured velocities from linear theory depends on the degree of wind forcing. Thus the accuracy of C_D and C_M will depend also on wind forcing and other causes of nonlinearity in the wave field.

4.4 Wave-turbulence interaction

Turbulence can be thought of as a process in which energy is transfered continuously from larger scales of motion to smaller ones. The source of turbulent energy is in the larger scales of motion – current shear or wave breaking, say – and the energy is eventually lost, in the smallest scales, through dissipation into heat. One of the key parameters in a study of turbulence is the dissipation rate ϵ. In particular, it plays a key rôle in the energy balance equation: in the intermediate scales (the 'inertial subrange' – see below), the energy flux rate equals the dissipation rate, there being no sources or sinks of energy at these scales.

According to the classical work of Kolmogorov (see Monin and Yaglom, 1975, Chapter 21), in the case of flow with a sufficiently high Reynolds number in which the turbulence is locally isotropic (i.e. independent of spatial orientation), the probability distributions of the velocity fluctuations about some mean are dependent only on the dissipation rate and fluid viscosity. Furthermore, for certain scales of motion (restricted in both space and time), the probability distributions of the velocity fluctuations will be a function solely of the dissipation rate. These are known, respectively,

as Kolmogorov's first and second similarity hypotheses. The importance of the second hypothesis follows from an application of dimensional analysis in which it is shown that, where the hypothesis applies (i.e. in the inertial subrange), the velocity spectra E_{uu} and E_{ww} are of the form

$$E_{uu}(k) = C_1 \epsilon^{2/3} k^{-5/3} \qquad E_{ww}(k) = C_2 \epsilon^{2/3} k^{-5/3}, \tag{4}$$

where k is the wavenumber. Consequently, spectral values in the inertial subrange can be used to provide dissipation estimates. (We use $C_1 = C_2 = 18/55$ - see Monin and Yaglom, 1975).

Although the spectra above are wavenumber spectra, time series yield *frequency* spectra, so that the above relations are not strictly applicable to most measurements. If, however, the magnitude of turbulent energy is considerably less than that associated with the principal motion (due to waves, currents or the convection velocity associated with a moving probe), then Taylor's frozen turbulence hypothesis can be invoked to convert temporal variation to spatial variation. Essentially this hypothesis states that we can think of the turbulent eddies being convected so quickly past the measuring probe by the principal motion that the turbulence appears to be frozen in time. Consequently, variations in space appear as variations in time: $k = 2\pi f / U_D$, where U_D is a measure of this 'drift velocity' past the probe, and the frequency and wavenumber spectra, $S(f)$ and $E(k)$ respectively, are related according to $S(f) = \frac{2\pi}{U_D} E(2\pi f / U_D)$.

From the point of view of the drag sphere measurements (see Figure 5) there is often evidence of an inertial subrange at frequencies greater than 1-2 Hz. The energy present at these scales is typically several orders of magnitude less than that present around the peak wave frequencies (0.1 - 0.5 Hz.), allowing for Taylor's hypothesis to be applied. We note here that the convection velocity associated with wave orbital motion is, of course, not steady in time, so that a time series of equally spaced points

will yield, under Taylor's hypothesis, a spatial series with unequally spaced points. Several of these space series were then resampled – using Fourier interpolation – so as to arrive at evenly spaced series, for which analysis techniques were readily available. It was found that, over most of the inertial subrange, this resulted in no change in the spectral values (see Figure 16). Consequently, the time intensive step of Fourier interpolation was generally omitted.

Over the past decades, several researchers have made measurements of dissipation rates in the ocean. Measurements have been made from fixed towers (e.g. Kitaigorodskii *et al.*, 1983), using free-rising or free-falling probes (e.g. Soloviev *et al.*, 1988) and from moving vessels (e.g. Stewart and Grant, 1962). Most of these results, summarized by Soloviev *et al.* (1988), indicate that dissipation scales according to $\epsilon \propto u_*^3/z$, where u_* is the friction velocity, which is proportional to the wind speed (we use $u_* = 0.0012 \times U_{12}$ – see Kitaigorodskii *et al.*, 1983). This dissipation rate is commensurate with turbulence derived from current shear alone – classical 'law of the wall' turbulence. It is not, however, supported by all of the data. Kitaigorodskii *et al.* (1983) report dissipation measurements several orders of magnitude higher than 'law of the wall' scaling would suggest. These measurements, taken in strongly forced, fetch limited conditions, indicate that the simple current shear model is inappropriate – other sources of turbulent energy (i.e. wave breaking) must be taken into account.

Table 3 provides a summary of the dissipation results from the WAVES 85 data set. Independent estimates of dissipation were made from both $S_{uu}(f)$ and $S_{ww}(f)$ for all cases in which an inertial subrange was detected. These dissipation estimates are generally based on the high frequency inertial subrange, with convection past the drag sphere at the wave orbital velocity. We note that Kitaigorodskii *et al.* (1983) based their findings on the lower frequency inertial subrange (at frequencies lower than the wave peak), with convection at the mean current velocity. In the WAVES 85 data set,

there were only four cases which had both a low frequency inertial subrange and a mean current (drift velocity) of sufficient magnitude for Taylor's hypothesis to be applied : they are also included in Table 3. Plotted in wall layer coordinates in Figure 17 are dissipation values from WAVES 1985, along with those summarized in Soloviev *et al.* (1988). Clearly the two data sets are from different populations. In Table 4, which is modified from Soloviev *et al.* (1988), we summarize the conditions present during the various experiments whose data make up Figure 17. Note that the data which follow wall layer scaling are measured at low wind speeds and/or at depths of 5 metres or greater with run lengths typically of the order of seconds or minutes. The Lake Ontario data (Kitaigorodskii *et al.* (1983) and the WAVES experiments), with runs typically over an hour in length, however, are taken near the surface, often in conditions of high wind speed. In these conditions, wave breaking, although still intermittent, would be important and would show up in long enough (in time) records as increased dissipation. Recent results of Gregg (1987) support this interpretation.

We note here that the above is a brief summary of the WAVES results relating to wave-turbulence interaction. These results will be elaborated upon in an upcoming NWRI report and in journal publications.

5. CONCLUSIONS

The data collected during the WAVES experiments, covering a wide range of meteorological conditions, indicate that linear theory, based on wave height data, is able to predict flow velocities to within about 10%. The agreement between measured and predicted spectral values is very good in the vicinity of the peak of the spectrum, with discrepancies observed at higher frequencies. As was noted, however, these discrepancies, resulting from turbulence in the wave field, occur at energy levels one to two orders of magnitude below the peak values. Consequently, their effect on the

velocity comparison is minimal. With respect to horizontal velocities in wind-driven seas, it was found that a correction for directional spreading should be applied to the wave height spectrum prior to the implementation of linear theory. Otherwise, there is some evidence that the energy at frequencies several times the peak frequency will be overestimated.

Strong evidence was found indicating that the phase angle between horizontal and vertical velocities is very nearly 90°, as indicated by linear theory.

The drag forces $u|u|$ are quite well predicted by linear theory, although, as pointed out above larger trough forces tend to be underestimated and crest forces overestimated due to the effects of finite wave height. We note here that currents have not been taken into account in the analysis, with the measured velocities being detrended. It is, however, important to note that currents will affect the underlying velocity field – particularly the horizontal velocities – in a way which linear theory does not account for. In particular, they will have a direct impact on the loading on a object. Whether or not the incremental forces due to currents are large compared with the loadings associated with extreme wave crests will depend on particular conditions.

Given the importance of local accelerations on the inertial forces, it is perhaps not surprising that linear theory, which ignores flow turbulence, severely underestimates these forces. However, as was noted above, the inertial coefficient C_M is empirically determined with these limitations – i.e. linear theory is typically used to obtain wave velocities, whereas the actual wave forces on a cylinder (say) are measured directly – so that Morison's equation may still provide valid force estimates. In employing Morison's equation, it is very important that the drag and inertial coefficients C_D and C_M to be used were determined under similar conditions to those of the intended application. The coefficients are by no means universal.

The high frequency turbulence measurements yielded by the drag spheres have provided a unique data set for the study of turbulent dissipation. It has been found that under strongly forced conditions (i.e. high winds) there is a region of enhanced energy dissipation close to the surface. This finding is in contrast to the 'wall layer' dissipation estimates determined by others in calmer conditions, and has important implications for mixing processes at the air-sea interface.

ACKNOWLEDGEMENTS

Many members of the staff of the National Water Research Institute contributed to this study. We acknowledge, in particular, D. Beesley and R. Desrosiers. This experiment was supported in part by the Panel on Energy Research and Development under PERD project number 62123. K.K. Kahma and W.M. Drennan would like to thank the National Water Research Institute for its hospitality while this work was carried out.

REFERENCES

Arsenyev, S.A., Dobroklonskiy, S.V., Mamedov, R.M. and Shelkovnikov, N.K., (1975), 'Direct measurements of small-scale marine turbulence characteristics from a stationary platform in the open sea', *Izv., Atmos. and Oceanic Phys.* **11**, 530-533.

Battjes, J.A. and van Heteren, J. (1984), 'Verification of linear theory for particle velocities in wind waves based on field measurements', *Appl. Ocean Res.* **6**, 187-196.

Bearman, P.W., Chaplin, J.R., Graham, J.M.R., Kostense, J.K., Hall, P.F. and Klopman, G. (1985), 'The loading on a cylinder in post-critical flow beneath periodic and random waves', in *Behaviour of offshore structures*, Elsevier Scientific Pub. B.V., Amsterdam, 213-225.

Bendat, J.S. and Piersol, A.G. (1971), *Random data: analysis and measurement procedures*, Wiley-Interscience, New York, USA.

Cavaleri, L., Ewing, J.A. and Smith, N.D. (1977), 'Measurement of the pressure and velocity field below surface waves', in *Turbulent fluxes through the sea surface, wave dynamics and prediction* (eds. Favre, A. and Hasselmann, K.), Plenum Press, New York, 257-272.

Cavaleri, L. and Zecchetto, S. (1987), 'Reynolds stresses under wind waves', *J. Geophys. Res.* **92 C4**, 3894-3904.

Dillon, T.M, Richman, J.G., Hansen, C.G. and Pearson, M.D. (1981) 'Near-surface turbulence measurements in a lake', *Nature* **290**, 390-392.

Donelan, M.A., Anctil, F. and Doering, J.C. (1991), 'A simple method for calculating the velocity field beneath irregular waves', *Coastal Engng.* (in press).

Donelan, M.A., Hamilton, J. and Hui, W.H. (1985), 'Directional spectra of wind-generated waves', *Phil. Trans. R. Soc. London* **A315**, 509-562.

Donelan, M.A. and Kahma, K.K. (1987), 'Observations of velocities beneath wind-driven waves', in *Proc. First Int'l. Workshop on Wave Hindcasting and Forecasting*, Halifax, 243-252.

Donelan, M.A. and Motycka, J. (1978), 'Miniature drag sphere velocity probe', *Rev. Sci. Instrum.* **49**, 298-304.

Forristall, G.Z., Ward, E.G, Cardone, V.J. and Borgmann, L.E. (1978), 'The directional spectra and kinematics of surface gravity waves in tropical storm Delia', *J. Phys. Ocean.* **8**, 888-909.

Gregg, M.C. (1987), 'Structures and fluxes in a deep convecting mixed layer', in *Dynamics of the oceanic surface mixed layer*, (eds. Muller, P. and Henderson, D.), 1-23.

Guza, R.T. and Thornton, E.B. (1980), 'Local and shoaled comparisons of sea surface elevations, pressures and velocities', *J. Geophys. Res.* **85 C3**, 1524-1530.

Harris, F.J. (1978), 'On the use of windows for harmonic analysis with the discrete Fourier transform', *Proc. IEEE* **66**, 51-83.

Jefferys, E.R. (1986), 'Comparison of three methods for calculation of directional spectra', in *Proc. 5th Int'l. Offshore Mechanics and Arctic Engng. Symp.*, Tokyo, Japan, Vol. 1, 45-50.

Kitaigorodskii, S.A., Donelan, M.A., Lumley, J.L. and Terray, E.A. (1983), 'Wave-turbulence interactions in the upper ocean. Part II: Statistical characteristics of wave and turbulent components of the random velocity field in the marine surface layer', *J. Phys. Ocean.* **13**, 1988-1999.

Melville, W.K. and Rapp, R.J. (1985), 'Momentum flux in breaking waves', *Nature* **317**, 514-516.

Monin, A.S. and Yaglom, A.M. (1975), *Statistical Fluid Mechanics II*, MIT Press, Cambridge, Mass., USA

Morison, J.R., O'Brien, M.P., Johnson, J.W. and Schaaf, S.A. (1950), 'The force exerted by surface waves on piles', *Petroleum Trans., AIME* **189**, 149-154.

Oakey, N.S. and Elliott, J.A. (1982), 'Dissipation within the surface mixed layer', *J. Phys. Ocean.* **12**, 171-185.

Ramberg, S.E. and Niedzwecki, J.M. (1979), 'Some uncertainties and errors in wave force computations', in *Proc. 11th Offshore Technology Conference*, Houston (OTC 3597), 2091-2101.

Sarpkaya, T. and Isaacson, M. (1981), *Mechanics of wave forces on offshore structures*, Van Nostrand Reinhold Company, New York, USA

Shonting, D.H. (1970), 'Observations of Reynolds stresses in wind waves', *Pure & Appl. Geophys.* **81**, 202-210.

Simpson, J.H. (1969), 'Observations of the directional characteristics of sea waves', *Geophys. J. Royal Astron. Soc.* **17**, 93-120.

Soloviev, A.V., Vershinsky, N.V. and Bezverchnii, V.A. (1988), 'Small-scale turbulence measurements in the thin surface layer of the ocean', *Deep-sea Research* **35**, 1859-1874.

Stewart, R.W. and Grant, H.L. (1962), 'Determination of the rate of dissipation of turbulent energy near the sea surface in the presence of waves', *J. Geophys. Res.* **67**, 3177-3180.

Thornton, E.B. and Krapohl, R.F. (1974), 'Water particle velocities measured under ocean waves', *J. Geophys. Res.* **79**, 847-852.

Tsanis, I.K. and Donelan, M.A. (1989), 'Wave directional spectra in mixed seas', in *Proc. Second Int'l. Workshop on Wave Hindcasting and Forecasting*, 387-396.

Vis, F.C. (1980), 'Orbital velocities in irregular waves', *Waterloopkundig laboratorium* **231**, Delft hydraulics laboratory, Delft, The Netherlands.

LIST OF TABLES AND FIGURES

Figure 12: Joint frequency distributions of u and u_l, w and w_l.

Figure 13: Time series of $u|u|$ (—) and $u_l|u_l|$ (- -).

Figure 14: Time series of $\dot{u}$ (—) and $\dot{u}_l$ (- -).

Figure 15: Joint frequency distributions of $u|u|$ and $u_l|u_l|$.

Figure 16: Spectra of turbulent component of vertical velocity, run 87091, with (—) and without (- -) Fourier interpolation. Turbulent component is obtained after removing wave-coherent component through filtering. (See Kitaigorodskii *et al.*, 1983).

Figure 17: Dissipation in 'wall layer' coordinates $\epsilon\kappa z/u_*^3$ versus zg/u_*^2. The 'law of the wall' appears as the vertical line (—). (ref. Soloviev *et al.*, 1988)

Table 1: Summary of WAVES 85 & 87 runs.

Run	Julian date	GMT time	length (min)	Wind dir (deg)	U_{12} (m/s)	T_a (°C)	T_w (°C)	H_s (m)
85101	318	12.27	80.0	38	5.78	5.67	8.96	0.74
85102	319	11.27	65.5	26	4.74	0.97	8.73	0.54
85103	319	13.10	80.0	37	5.01	1.45	8.80	0.50
85104	319	17.26	80.0	63	6.68	2.27	8.76	0.50
85105	320	09.34	47.0	87	10.54	1.34	8.02	1.87
85106	320	11.51	80.0	91	9.13	3.19	7.94	1.93
85107	320	13.48	80.0	96	7.13	4.76	7.84	1.89
85108	320	16.45	80.0	107	1.95	6.41	7.81	1.71
85109	322	12.07	40.0	67	2.95	7.92	8.17	0.16
85110	322	19.10	61.5	61	4.14	8.34	8.12	0.72
85111	322	20.59	80.0	134	0.84	8.70	8.63	0.73
85112	323	18.21	14.5	220	3.10	16.98	9.10	0.12
85113	323	18.50	49.0	196	3.78	15.90	9.10	0.12
85114	324	06.33	49.5	259	10.67	11.48	9.00	0.29
85115	324	07.36	40.5	267	10.04	8.23	8.97	0.29
85116	324	09.17	58.5	241	10.73	6.58	8.97	0.27
85117	324	12.04	80.0	242	10.43	6.81	8.99	0.26
85118	324	14.31	80.0	245	10.23	6.05	8.97	0.24
85119	324	16.15	100.0	248	8.26	4.77	8.91	0.19
85120	324	19.55	20.0	262	8.66	2.73	8.80	0.19
85121	325	22.41	14.0	12	6.13	0.97	8.46	0.33
85122	325	22.58	16.0	13	5.92	1.13	8.46	0.33
85123	326	08.19	5.0	89	14.21	3.23	8.18	1.78
85124	326	08.29	16.5	86	16.03	3.07	8.09	1.82
85125	326	08.53	80.0	90	17.18	1.38	7.91	2.03
85126	326	14.03	80.0	96	5.06	1.88	7.68	1.76
85127	326	14.03	21.5	71	2.00	2.19	7.96	1.32
85128	326	16.27	55.0	13	4.11	1.72	8.06	1.31
85129	326	17.36	88.0	337	5.24	0.11	8.12	1.13
85131	327	02.04	43.0	227	6.87	2.71	7.93	0.42
85132	327	17.04	40.0	193	2.59	4.04	7.72	0.05
85133	329	14.24	60.0	57	2.46	1.69	7.35	0.09
85134	329	15.40	80.0	70	3.57	1.82	7.31	0.11
85135	329	21.31	60.0	112	8.01	1.52	7.19	0.62
85136	330	09.46	80.0	91	6.50	2.25	6.89	1.39
85137	330	20.52	60.0	52	7.29	2.84	6.59	1.43
85138	330	22.47	23.5	51	6.06	2.51	6.44	1.35
85139	330	23.15	25.0	43	5.74	2.38	6.45	1.34
85140	330	23.42	46.0	13	4.74	1.58	6.50	1.30
85141	331	02.23	80.0	243	1.21	1.38	6.64	0.97
85142	331	04.14	13.0	314	2.07	1.64	7.12	0.93
85143	331	04.33	65.0	5	2.98	1.71	7.32	0.78
85144	332	09.45	60.0	64	14.24	1.26	6.40	2.40
85145	332	10.46	80.0	67	13.98	1.22	6.65	2.31
85157	334	15.22	80.0	41	2.48	4.28	6.41	0.98
85158	335	09.58	80.0	53	1.65	6.55	6.58	0.59
85159	336	02.45	80.0	234	16.00	2.47	6.73	0.49
85160	336	06.32	80.0	230	12.74	-2.86	6.55	0.32
85161	336	12.54	120.0	263	14.36	-5.04	6.20	0.46

Run	Julian date	GMT time	length (min)	Wind dir (deg)	U_{12} (m/s)	T_a (°C)	T_w (°C)	H_s (m)
87001	290	16.10	90.0	217	6.71	-7.60	7.15	0.12
87002	290	18.16	5.5	213	6.14	-6.50	7.35	0.11
87003	290	18.32	10.0	200	6.41	-6.45	7.32	0.11
87004	293	18.15	90.0	355	4.78	0.07	6.55	0.51
87005	293	20.38	7.0	352	5.22	-0.22	6.52	0.49
87006	299	21.23	4.5	254	6.45	9.04	5.76	0.13
87007	302	04.06	15.0	229	2.19	3.89	6.14	0.05
87008	302	04.55	15.0	213	1.67	4.38	6.14	0.05
87009	302	05.29	15.0	196	1.40	4.06	6.14	0.04
87010	302	05.56	15.0	188	1.55	4.15	6.13	0.04
87011	302	06.33	15.0	241	1.46	4.70	6.17	0.04
87012	302	20.50	5.0	247	6.07	7.59	6.41	0.17
87013	302	20.58	15.0	266	6.92	8.34	6.41	0.15
87014	303	18.47	40.0	198	6.38	12.08	6.51	0.15
87015	306	21.52	95.0	20	3.25	7.61	7.12	0.78
87016	308	21.50	33.0	250	6.42	18.17	7.34	0.12
87017	308	22.54	95.0	254	6.51	17.19	7.36	0.12
87018	309	00.48	95.0	240	5.95	16.22	7.39	0.10
87019	309	17.27	10.0	274	7.97	7.44	7.73	0.21
87020	309	18.50	21.0	300	10.77	6.37	7.70	0.35
87021	309	20.27	95.0	292	11.66	5.39	7.64	0.39
87022	309	22.41	95.0	303	9.85	2.91	7.68	0.34
87023	310	01.48	95.0	295	8.55	1.22	7.81	0.31
87024	310	04.14	31.0	324	6.18	-0.40	7.46	0.23
87025	310	22.51	95.0	243	8.00	3.06	7.23	0.18
87026	311	01.48	15.0	230	6.16	2.90	6.99	0.13
87028	311	02.04	95.0	239	6.66	4.08	7.08	0.13
87029	312	02.11	54.0	220	3.49	7.36	7.08	0.07
87030	312	16.13	91.5	243	6.59	12.63	7.18	0.13
87031	312	19.06	36.0	251	5.08	13.01	7.16	0.09
87032	313	18.40	30.5	25	4.78	3.87	7.14	0.34
87033	314	03.09	57.5	2	4.44	-0.06	6.97	0.36
87034	314	12.54	32.5	66	5.97	0.00	6.82	0.49
87035	314	15.25	14.0	74	7.73	-0.09	6.78	0.74
87036	314	16.16	21.0	59	7.29	-0.13	6.76	0.84
87037	314	18.10	95.0	45	5.43	-0.15	6.75	0.73
87038	314	21.24	95.0	26	7.26	0.45	6.71	0.64
87039	315	00.40	95.0	359	7.31	-0.44	6.70	0.68
87040	315	14.40	70.5	5	3.56	-1.70	6.38	0.82
87041	315	19.32	28.0	93	1.49	2.82	6.72	0.67
87042	315	22.04	34.5	285	5.05	2.33	6.61	0.54
87043	315	23.27	15.0	284	4.11	2.13	6.52	0.48
87044	315	23.50	95.0	245	3.29	1.64	6.45	0.38
87045	316	13.29	95.0	255	6.69	3.63	6.26	0.17
87046	316	19.26	60.0	328	2.86	7.22	6.29	0.10
87047	316	21.02	95.0	242	4.77	8.01	6.24	0.10
87048	316	23.12	95.0	208	2.65	5.10	6.17	0.04
87049	317	17.25	75.0	233	8.53	12.57	6.77	0.18
87050	317	19.02	46.5	233	8.90	12.88	6.81	0.19

Run	Julian date	GMT time	length (min)	Wind dir (deg)	U_{12} (m/s)	T_a (°C)	T_w (°C)	H_s (m)
87051	317	20.54	95.0	233	7.85	10.98	6.68	0.16
87052	318	16.01	93.0	297	4.15	9.05	6.83	0.14
87053	319	17.40	27.5	67	4.14	7.51	6.89	0.39
87054	319	18.12	32.0	63	4.06	7.51	6.88	0.44
87055	319	18.46	40.0	51	4.28	7.88	6.88	0.48
87056	319	20.21	95.0	42	4.36	7.04	6.85	0.65
87057	319	22.26	38.5	45	3.38	7.05	6.83	0.78
87058	319	23.11	57.5	46	3.80	7.07	6.83	0.83
87059	320	02.58	59.5	24	4.02	6.49	6.78	0.85
87060	320	03.59	40.0	11	3.96	6.18	6.77	0.83
87061	320	05.51	95.0	15	2.13	5.74	6.74	0.75
87062	320	07.51	95.0	356	2.68	4.89	6.72	0.74
87063	320	11.01	32.5	337	1.67	3.99	6.69	0.66
87064	320	11.42	58.0	350	1.54	3.99	6.68	0.64
87065	320	16.60	44.5	60	0.49	7.18	6.81	0.46
87066	320	21.46	95.0	19	3.14	6.88	6.89	0.40
87067	321	01.40	76.0	21	2.92	7.37	6.79	0.38
87068	321	03.58	15.0	286	1.30	11.43	6.76	0.36
87069	321	04.16	15.0	311	0.81	10.92	6.76	0.33
87070	321	04.33	15.0	315	1.25	10.68	6.76	0.36
87071	321	04.51	15.0	328	1.56	10.47	6.75	0.38
87072	321	05.08	15.0	189	2.14	11.51	6.75	0.37
87073	321	05.25	15.0	182	2.61	12.08	6.74	0.37
87074	321	11.47	95.0	179	8.41	15.22	6.60	0.35
87075	321	15.29	95.0	181	8.13	15.63	6.64	0.28
87076	321	17.50	95.0	183	10.06	16.30	6.71	0.36
87077	322	00.14	9.5	193	8.29	14.64	7.09	0.24
87078	322	00.26	77.5	205	8.01	14.48	7.05	0.22
87079	322	03.03	95.0	231	7.01	14.77	7.06	0.16
87080	322	04.60	95.0	228	7.71	12.76	7.02	0.17
87081	322	08.15	95.0	231	8.99	10.95	6.93	0.19
87082	322	10.21	91.0	238	11.13	9.03	6.84	0.25
87083	322	13.00	7.5	239	11.90	8.04	6.77	0.30
87084	322	13.10	10.0	241	12.15	7.91	6.78	0.30
87085	322	13.36	9.0	234	10.95	7.56	6.75	0.27
87086	322	13.47	90.0	238	12.05	7.81	6.76	0.29
87087	322	17.37	95.0	246	11.41	7.89	6.73	0.28
87088	322	19.49	95.0	266	9.21	6.42	6.74	0.23
87089	323	13.00	95.0	229	7.65	4.31	6.42	0.15
87090	323	17.53	7.0	216	12.35	7.48	6.58	0.34
87091	323	18.05	95.0	221	11.54	7.62	6.58	0.28
87092	323	19.50	30.5	218	11.76	7.28	6.57	0.28
87093	324	14.17	95.0	335	6.96	-0.99	6.16	0.31
87094	324	16.12	91.5	338	6.88	-0.53	6.03	0.37
87095	324	20.56	38.0	330	6.61	-2.47	5.90	0.47
87096	324	21.36	30.0	322	6.50	-2.69	5.89	0.45
87097	324	22.09	30.0	311	8.42	-3.04	5.88	0.43
87098	325	00.02	95.0	310	6.14	-4.26	5.78	0.26
87099	325	02.56	30.0	6	10.39	-6.98	5.71	0.44
87100	325	03.30	30.0	6	10.35	-7.77	5.71	0.65

Run	Julian date	GMT time	length (min)	Wind dir (deg)	U_{12} (m/s)	T_a (°C)	T_w (°C)	H_s (m)
87101	325	04.04	30.0	2	11.13	-8.24	5.69	0.66
87102	325	07.30	4.5	344	7.28	-10.18	5.70	0.75
87103	325	07.36	28.5	337	5.53	-10.05	5.58	0.56
87104	325	08.52	85.5	345	5.24	-10.26	5.52	0.47
87105	325	10.43	30.0	315	3.44	-10.31	5.47	0.40
87106	325	11.25	30.0	311	4.34	-10.01	5.42	0.35
87107	325	19.25	95.0	333	6.86	-6.70	5.35	0.41
87108	326	00.55	95.0	291	6.93	-6.68	5.20	0.27
87109	326	03.03	95.0	319	5.14	-6.57	5.20	0.22
87110	327	18.05	10.0	204	8.62	8.59	5.18	0.23
87111	329	02.30	10.0	55	2.74	5.27	5.19	0.06
87112	329	02.48	95.0	47	3.75	5.04	5.19	0.12
87113	329	05.54	10.0	63	7.49	4.28	5.22	0.45
87114	329	14.39	95.0	67	12.74	3.19	5.14	2.09
87115	329	17.27	75.0	51	11.75	3.26	5.08	2.42
87116	329	21.25	95.0	52	10.27	3.07	5.07	2.32
87117	330	00.13	76.5	38	7.77	2.84	4.97	2.29
87118	330	02.40	35.0	17	7.16	1.42	4.96	1.95
87119	330	06.17	94.0	7	7.65	0.06	4.88	1.36
87120	330	09.27	69.5	13	8.02	0.13	4.75	1.19
87121	330	10.56	30.0	11	6.99	0.23	4.75	1.13
87122	330	11.45	30.0	4	7.86	-0.05	4.79	1.11
87123	330	12.30	30.0	7	7.67	-0.19	4.81	1.09
87124	330	13.14	30.0	14	6.28	-0.32	4.79	1.02
87125	330	14.20	95.0	12	5.44	-0.24	4.73	0.86
87126	330	18.26	30.0	62	4.59	1.21	4.73	0.68
87127	330	21.05	95.0	73	6.30	1.59	4.69	0.72
87128	331	13.07	95.0	80	9.67	2.23	4.52	1.37
87129	331	15.27	30.0	84	9.62	1.96	4.45	1.42
87130	331	15.59	30.0	77	9.39	1.99	4.46	1.42
87131	331	16.31	30.0	76	9.81	1.98	4.45	1.47
87132	331	19.00	95.0	76	10.38	0.88	4.47	1.71
87133	332	02.32	95.0	84	6.87	2.45	4.63	1.43
87134	332	14.10	95.0	82	5.57	4.62	4.29	1.07
87135	332	18.46	13.0	63	5.39	4.99	3.98	1.20
87136	332	19.06	10.0	55	6.04	5.02	3.99	1.28
87137	332	19.18	10.0	62	5.38	5.43	4.02	1.15
87138	332	19.31	30.0	60	5.25	5.36	4.02	1.21
87139	332	20.34	30.0	51	5.15	5.15	4.04	1.34
87140	332	21.18	95.0	56	2.16	4.95	4.16	1.26
87141	332	23.08	12.0	35	1.31	5.30	4.23	1.35
87142	332	23.23	95.0	63	1.63	5.40	4.20	1.16
87143	333	05.56	95.0	83	7.49	5.10	4.22	1.33
87144	333	07.53	95.0	85	4.80	4.99	4.13	1.36
87145	333	09.44	95.0	93	4.91	4.83	4.20	1.35
87146	333	15.25	95.0	75	3.94	5.49	4.30	1.10
87147	333	17.17	30.0	77	4.67	5.12	4.32	1.06
87148	333	17.49	30.0	90	3.94	5.24	4.33	0.98
87149	333	18.31	24.0	94	3.34	5.23	4.32	0.98
87150	334	03.15	10.0			5.76	4.21	0.62

Run	Julian date	GMT time	length (min)	Wind dir (deg)	U_{12} (m/s)	T_a (°C)	T_w (°C)	H_s (m)
87151	334	03.33	10.0			5.57	4.21	0.79
87152	334	19.54	46.0	222	7.03	5.02	4.29	0.15
87153	334	21.52	20.0	220	5.56	4.36	4.30	0.12
87154	335	18.14	75.0	354	4.41	0.27	4.22	0.26
87155	335	19.33	33.0	348	4.51	0.41	4.22	0.27
87156	336	15.40	75.0	250	6.78	0.42	4.29	0.15
87157	336	21.17	95.0	254	8.46	-0.04	4.23	0.21
87158	337	17.05	95.0	100	4.02	0.37	4.05	0.20
87159	337	19.11	82.0	112	4.57	1.00	4.02	0.27
87160	338	00.14	95.0	84	5.76	1.43	4.04	0.56
87161	338	03.16	95.0	53	8.13	1.58	4.01	0.65
87162	338	05.55	62.5	13	9.23	0.65	3.97	0.95
87163	338	08.59	49.5	12	9.92	-0.32	3.97	1.01
87164	338	10.55	95.0	7	8.40	-1.39	3.94	1.10
87165	338	13.18	95.0	0	7.87	-0.78	3.89	1.06
87166	338	16.13	60.0	350	7.05	0.37	3.88	0.88
87167	339	15.06	55.5	310	3.17	0.03	3.77	0.15
87168	339	16.04	40.0	349	2.38	0.22	3.78	0.11
87169	339	18.19	95.0	331	6.74	1.30	3.80	0.31
87170	342	18.09	95.0	3	1.06	3.99	3.81	0.24
87171	343	16.09	95.0	212	9.85	11.92	3.84	0.23
87172	343	18.40	95.0	226	11.25	12.82	3.94	0.26
87173	343	22.35	95.0	231	11.73	9.16	3.95	0.28
87174	344	01.25	95.0	225	9.30	7.39	3.97	0.21
87175	344	16.20	95.0	241	6.64	5.51	4.19	0.15
87176	344	19.03	95.0	210	4.73	5.35	4.20	0.09
87177	345	16.34	95.0	209	6.14	6.21	4.23	0.13
87178	345	18.20	77.5	199	6.88	5.79	4.24	0.16
87179	346	15.20	15.0	220	5.75	6.49	4.18	0.14
87180	346	15.40	64.5	213	7.70	6.68	4.18	0.19
87181	346	16.47	29.0	213	8.16	6.36	4.16	0.20
87182	346	18.47	27.0	219	9.15	5.73	4.23	0.21
87183	346	20.33	4.0	229	7.43	4.08	4.22	0.19
87184	346	20.40	65.0	245	9.71	2.85	4.21	0.21
87185	349	11.54	93.0	84	14.54	0.33		1.68
87186	349	13.31	29.0	82	15.81	0.56		2.00
87187	349	14.02	48.5	89	15.17	0.61		2.18
87188	349	14.53	66.0	81	14.07	0.86		2.37
87189	349	16.01	84.0	85	13.12	1.34		2.51
87190	349	20.18	35.0	240	9.50	2.74		1.88
87191	349	20.56	250.0	220	11.44	1.93		1.11
87192	350	02.18	38.5	210	12.45	0.91		0.53
87193	350	04.31	320.0	235	11.05	1.58		0.30

U_{12}-wind speed at 12 m.; T_a, T_w-air and water temperatures;
H_s-significant wave height (4 x r.m.s. wave height).

Table 2 : WAVES 85 – drag sphere results.

Run nr.	U_{12} (m/s)	θ_w (°)	D (°)	H_s (cm)	f_p (Hz)	U/c_p	depth (cm)	G_u	G_w	ϕ_{uw} (°)
85104	6.7	63	70	50	0.30	1.3	146 186 386	1.05 1.24 1.8	1.14 0.98 1.7	92 97
85105	10.5	87	75	187	0.14	0.9	158 198 398	0.94 1.08 1.11	0.91 0.98 1.01	91 98 92
85107	7.1	100	75	189	0.14	0.6	159 399	0.80 0.87	0.93 0.97	92 97
85111	0.9	var	55	73	0.20	0.1	151	1.07	1.07	89
85116	10.7	250	220	27	0.52	3.6	139	0.25	1.07	95
85117	10.4	250	220	26	0.53	3.5	140	1.10	1.23	97
85119	8.3	248	265	13	0.52	2.8	139	1.08	1.31	97
85125	17.2	90	80	203	0.17	1.9	164	0.70	1.01	89
85129	5.2	337		113	0.14	0.5	145	0.58	0.95	86
85135	8.0	112	75	62	0.30	1.5	120 390	0.88 1.17	0.95 1.37	89
85140	4.7	13	75	130	0.15	0.5	120 190 390	1.07 1.22 1.28	1.04 0.95 1.25	90 90
85144	14.2	64	75	240	0.14	1.3	132 202	0.90 1.10	0.89 0.88	93 93
85145	14.0	67	85	231	0.14	1.3	131 201 401	0.90 1.06 1.09	0.92 0.89 0.97	91 92 95
85159	16.0	234	240	49	0.41	4.2	104 174 401	1.08 1.10 1.90	1.07 1.13 1.95	88 85
85160	12.7	230	225	32	0.48	3.9	100 170	1.11 1.29	1.15 1.37	94 96

U_{12}, θ_w - wind speed and direction at 12 m.; D - wave direction;
H_s - 4 × r.m.s. wave height; f_p - frequency of wave peak;
U/c_p - wave age; ϕ_{uw} - phase angle between u and w at f_p;
G_u, G_w - variance gain, measured vs. linear theory;

Table 3 : Dissipation in WAVES 85.

Run nr.	z cm	U_D cm/s	U_{12} m/s	ϵ cm^2/s^3	zg/u_*^2 (x10^{-4})	$\kappa\epsilon z/u_*^3$
Dissipation based on high frequency w spectra						
85104	146	18.5	6.7	0.06	22.2	6.6
85104	186	15.5	6.7	0.02	28.2	2.8
85105	398	44.1	10.5	3.57	24.6	284.0
85107	159	62.2	7.1	11.3	21.5	1160.8
85107	399	46.5	7.1	6.78	53.9	1749.3
85111	151	27.7	0.9	0.04	1270.0	2154.7
85117	140	6.2	10.4	0.26	8.8	7.6
85125	164	61.2	17.2	27.99	3.8	208.8
85129	145	36.4	5.2	13.74	36.5	3280.5
85140	120	47.6	4.7	0.37	37.0	98.8
85145	401	58.0	14.0	4.26	13.9	144.2
85159	174	13.9	16.0	0.62	4.6	6.1
85160	100	13.6	12.7	0.61	4.2	6.9
Dissipation based on high frequency u spectra						
85104	146	18.5	6.7	0.09	22.2	9.7
85107	159	62.2	7.1	11.88	21.5	1221.8
85107	399	46.5	7.1	5.13	53.9	1323.6
85111	151	27.7	0.9	0.05	1270.0	2496.2
85125	164	61.2	17.2	32.05	3.8	239.1
85140	120	47.6	4.7	0.38	37.0	101.9
85140	190	42.4	4.7	0.12	58.6	50.6
85145	401	58.0	14.0	2.33	13.9	78.7
85159	174	13.9	16.0	0.39	4.6	3.8
85160	100	13.6	12.7	0.69	4.2	7.8
Dissipation based on low frequency u spectra						
85145	201	6	14.0	6.04	7.0	102.4
85159	104	5	16.0	0.36	2.8	2.1
85159	174	5	16.0	0.33	4.6	3.3
85160	100	5	12.7	0.14	4.2	1.6

$u_* = 0.0012 \times U_{12}$

Table 4 : Conditions during dissipation rate measurements †

Fig 17 symbol	Paper	Measurements	z (m)	U_{12} (m/s)	U_D (m/s)
×	Stewart *et al.* (1962)	from moving ship	1.5	6.0	1.5
◆	Arsenyev *et al.* (1975)	from fixed tower	6-15	6.0	0.04-0.08
+	Dillon *et al.* (1981)	free-rising probe	1.5	4.8	0.1
●	Oakey *et al.* (1982)	free-falling probe	8	6.5-14.1	0.5-0.6
○	Kitaigorodskii *et al.* (1983)	from fixed tower	0.44-0.62	10.7	0.11
△	Kitaigorodskii *et al.* (1983)	from fixed tower	0.67-1.17	11.2	0.08
□	Kitaigorodskii *et al.* (1983)	from fixed tower	0.82	5.8	0.03
●	Soloviev *et al.* (1988)	free-rising probe	0.2-5.8	1.9-6.0	2.2
■	this study	from fixed tower, based on low freq u	1-2	12.7-16.0	0.05-0.06
▼	this study	from fixed tower, based on high freq w	1-4	0.9-17.2	0.06-0.62
▲	this study	from fixed tower, based on high freq u	1-4	0.9-17.2	0.14-0.62

† Modified from Soloviev *et al.* (1988)

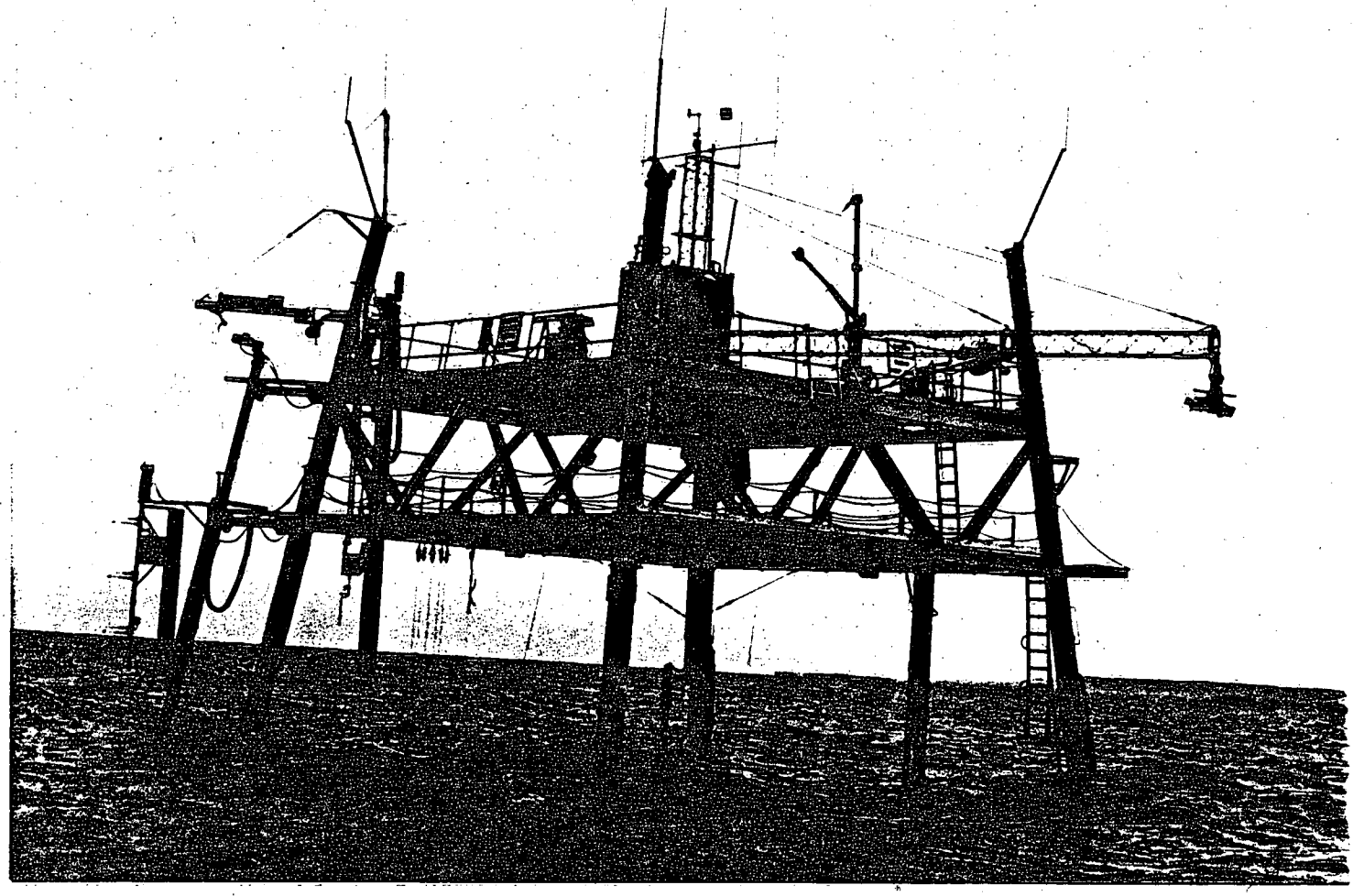

Figure 1: CCIW tower, Lake Ontario.

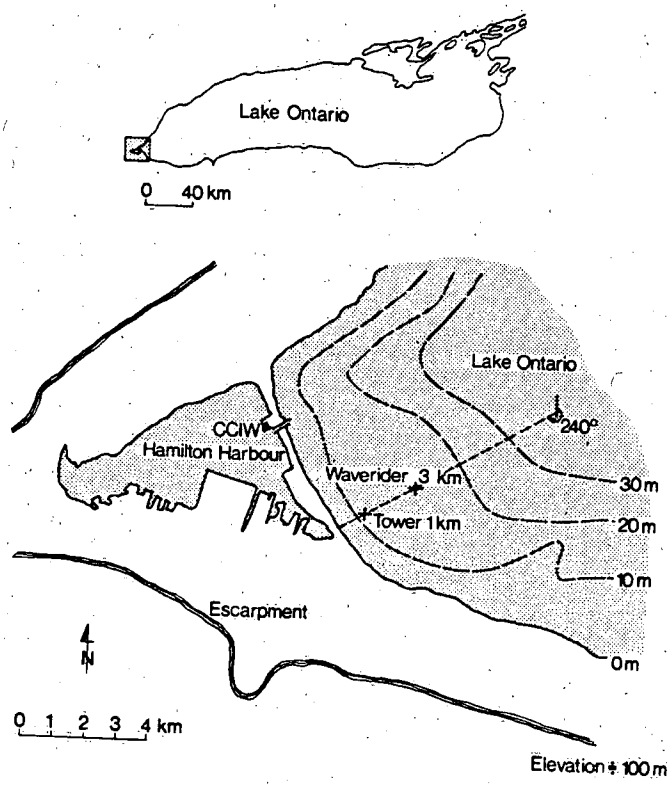

Figure 2: Map indicating tower location.

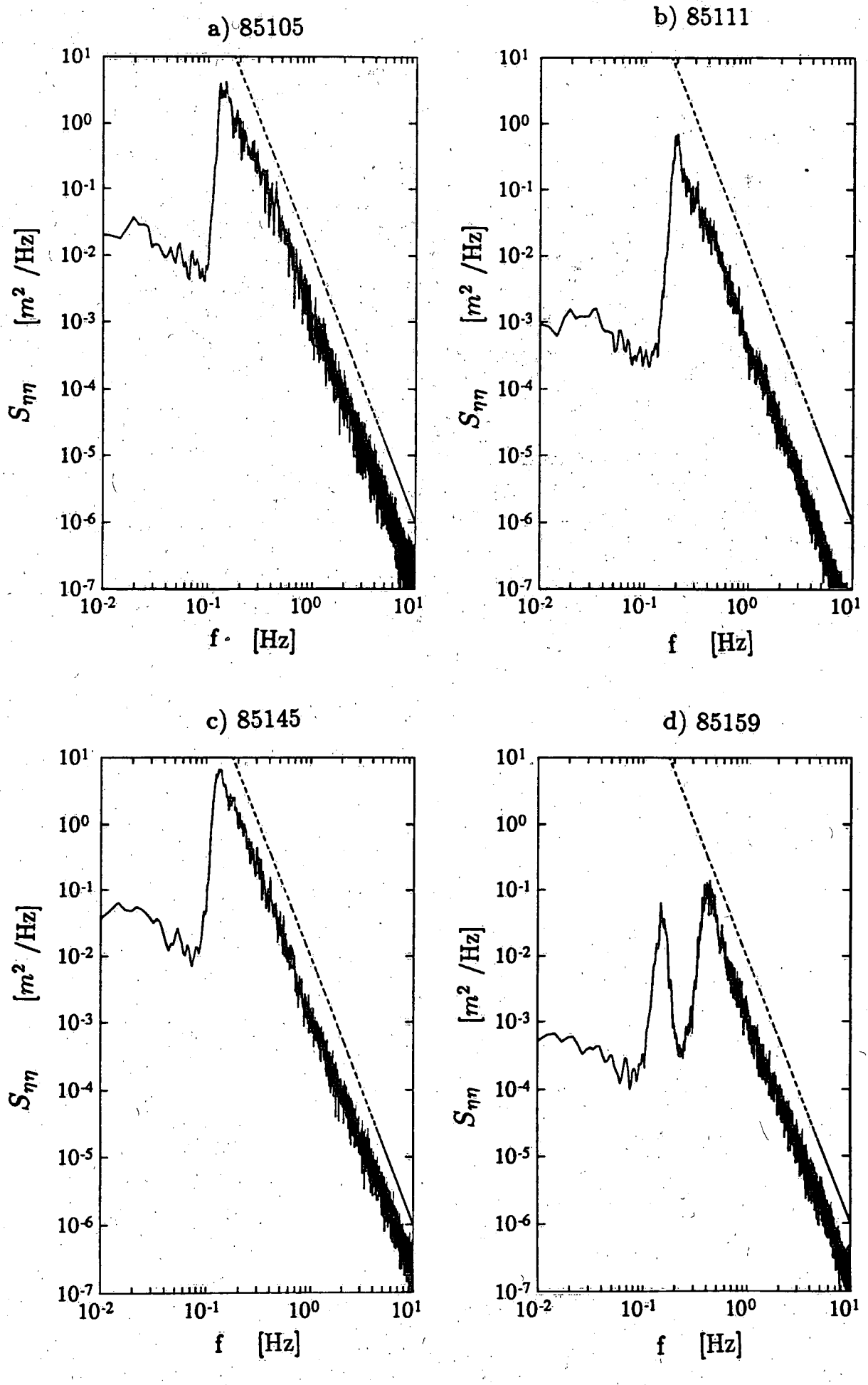

Figure 3: Wave height spectra $S_{\eta\eta}$, showing f^{-4} reference (- -).

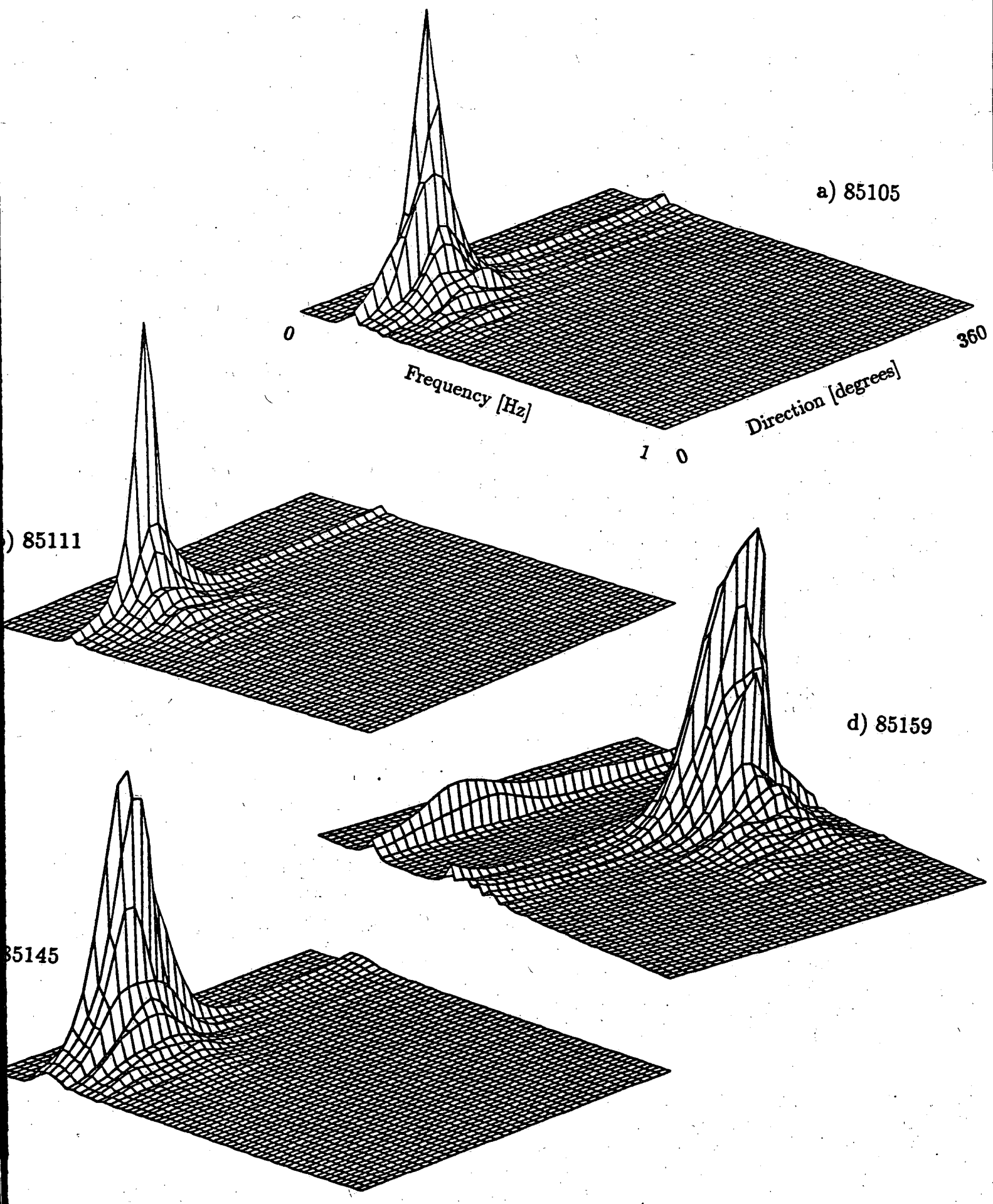

Figure 4: Directional spectra.

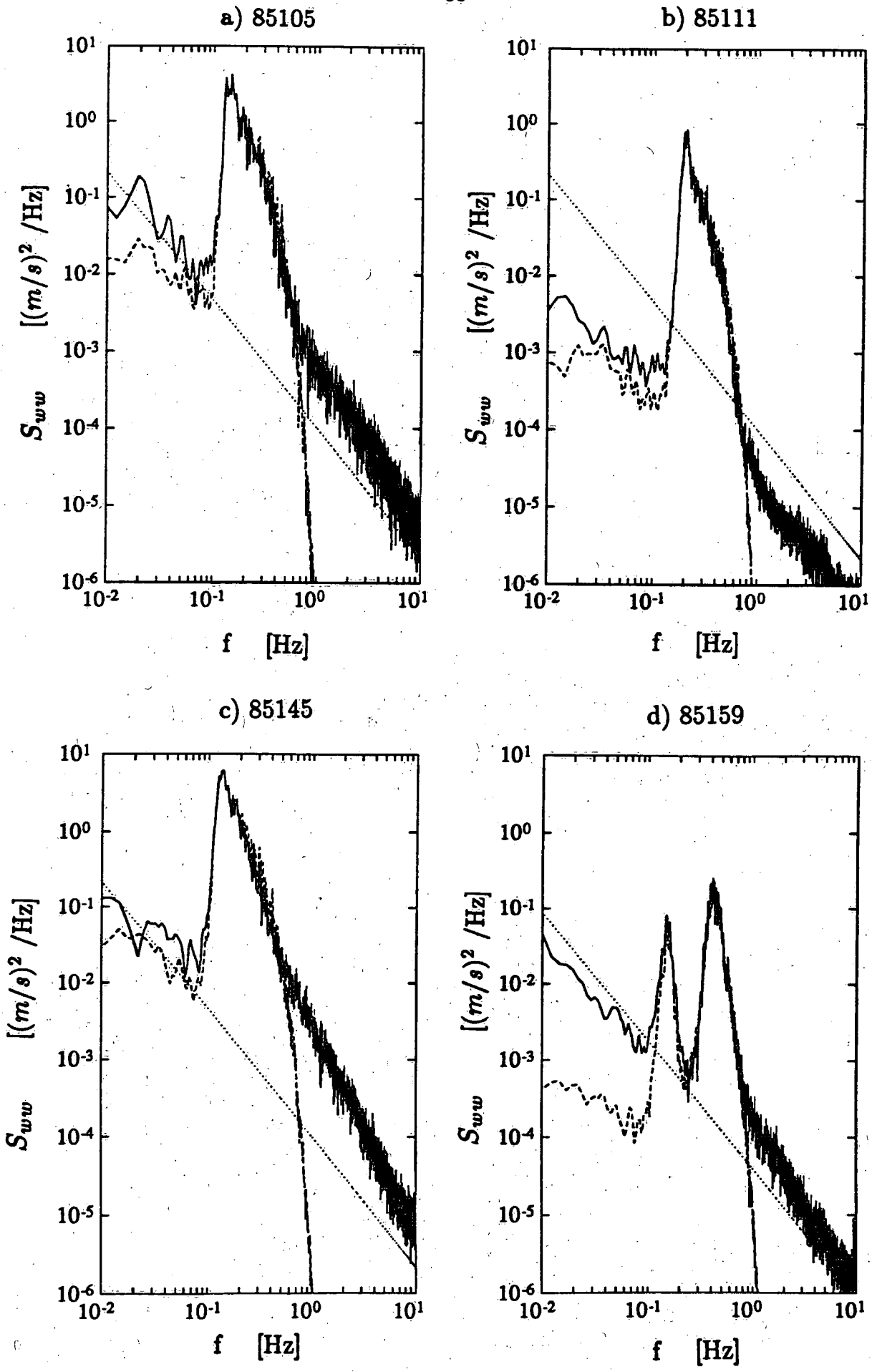

Figure 5: Vertical velocity spectra, S_{ww} measured (—) and via linear theory (- -), showing $f^{-5/3}$ reference slope ($\cdots$).

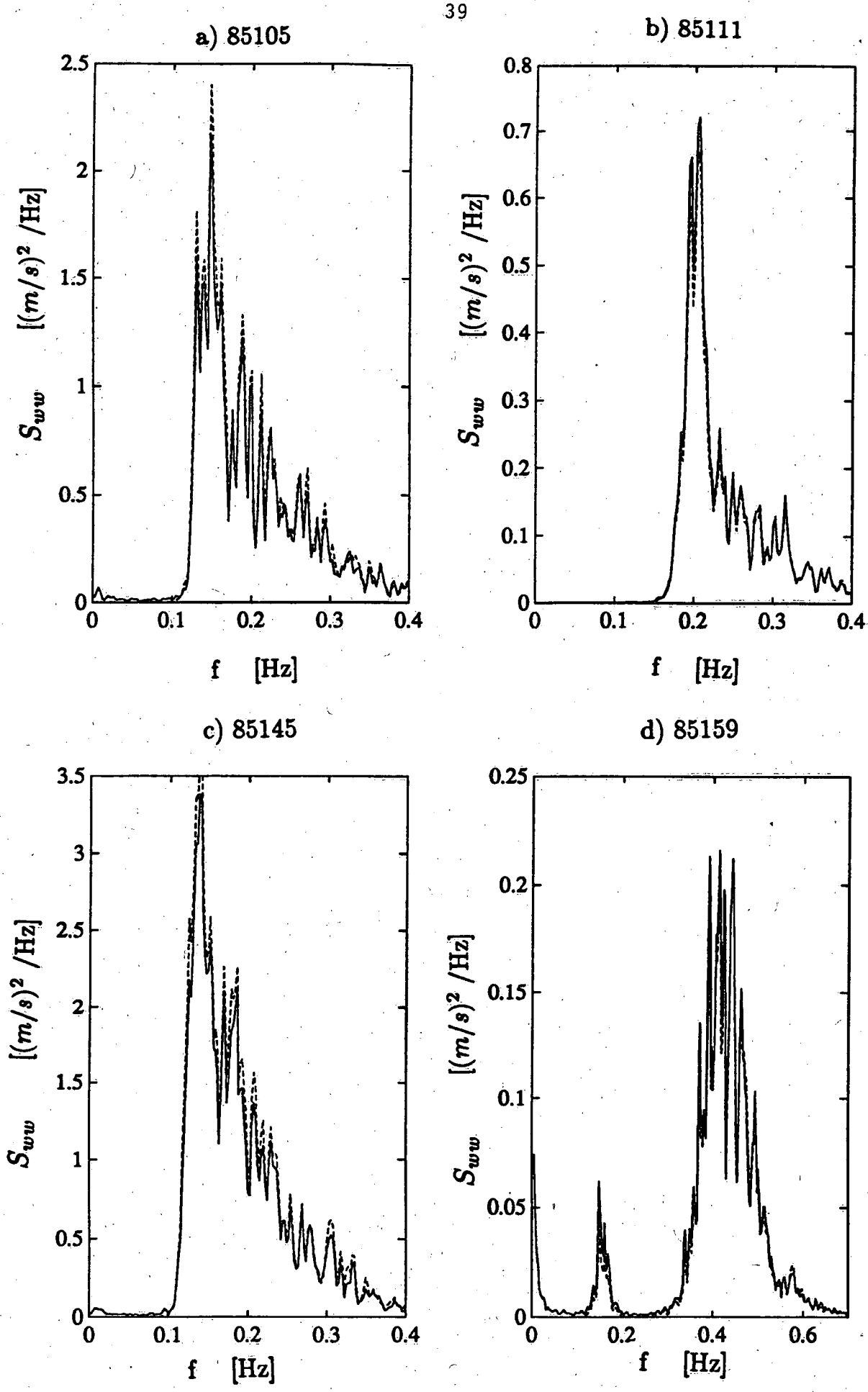

Figure 6: Vertical velocity spectra, S_{ww}, measured (—) and via linear theory (- -).

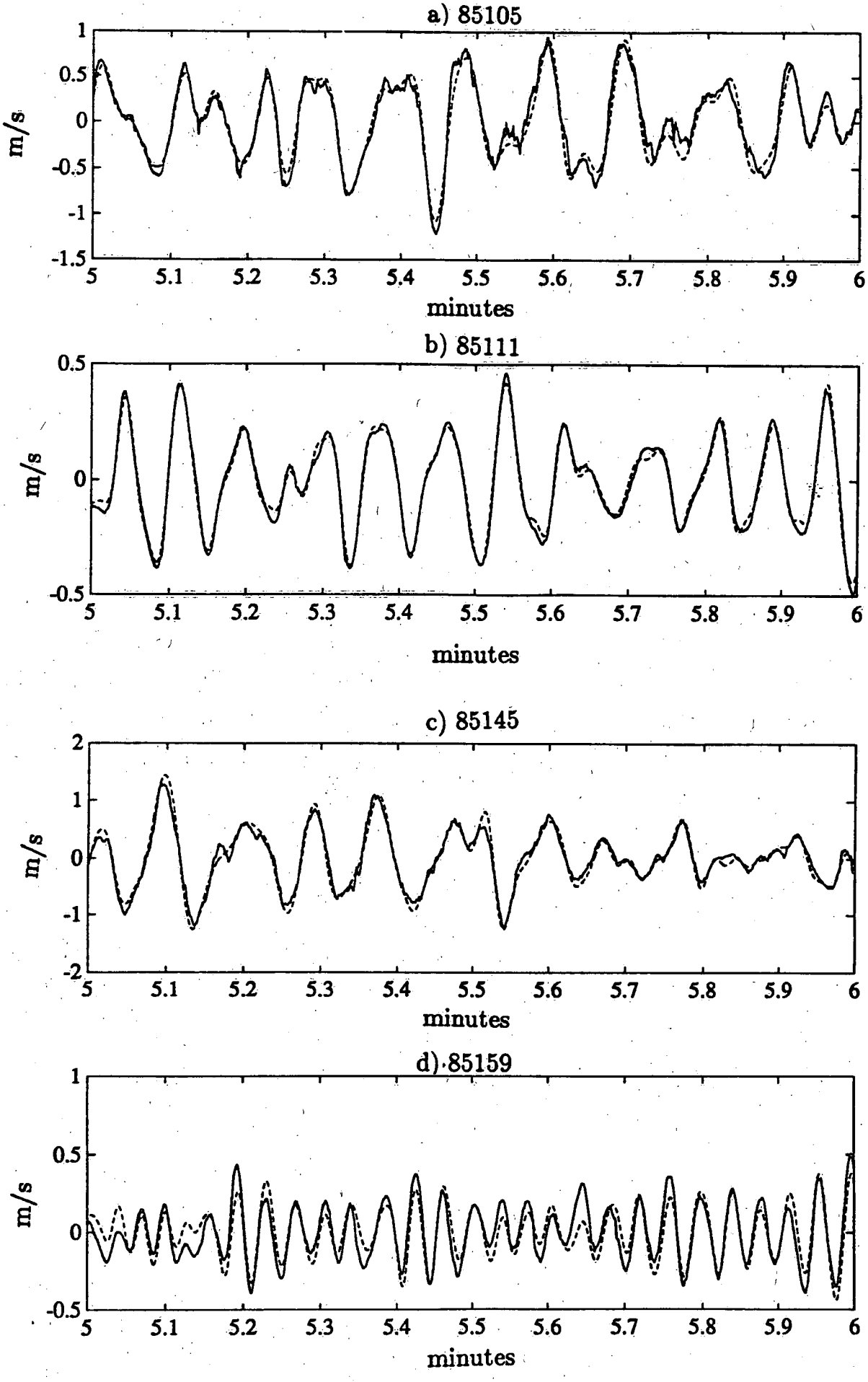

Figure 7: Time series of vertical velocity w, measured (—) and via linear theory (- -).

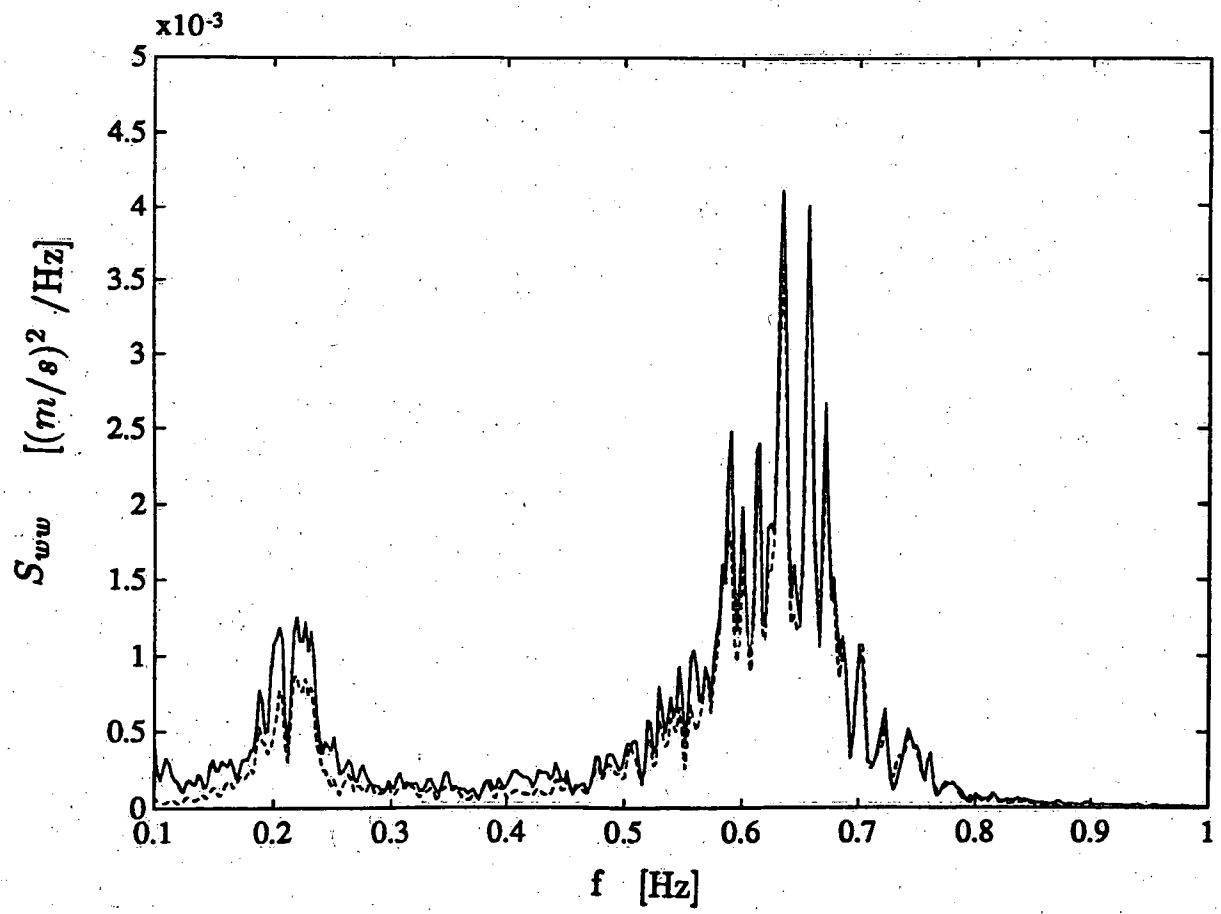

Figure 8: Vertical velocity spectrum S_{ww} for run 85119, measured (—) and via linear theory (- -).

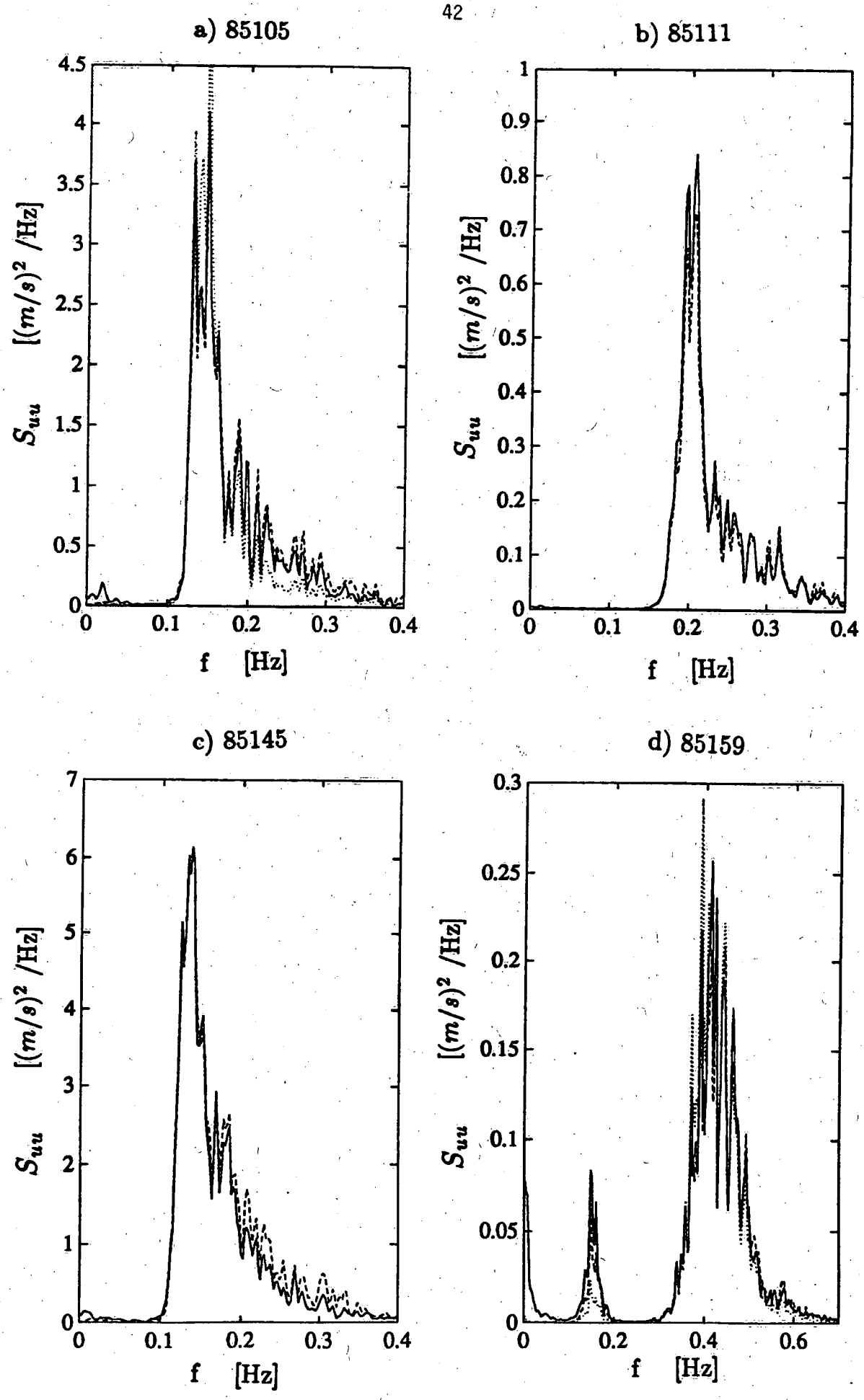

Figure 9: Horizontal velocity spectra, S_{uu}, measured (—) and via linear theory (- -). Corrected for directional spreading ($\cdots$).

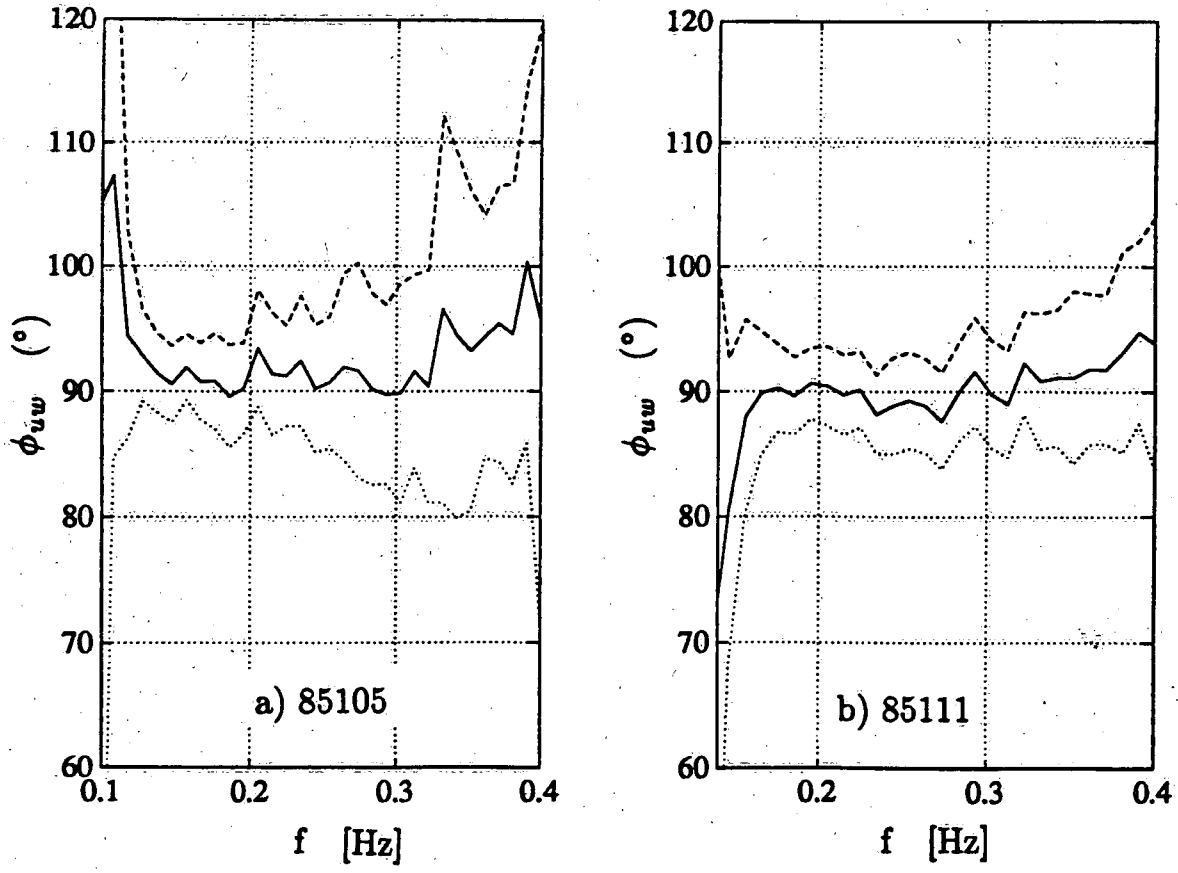

Figure 10: Phase angle between horizontal and vertical velocities, ϕ_{uw}.

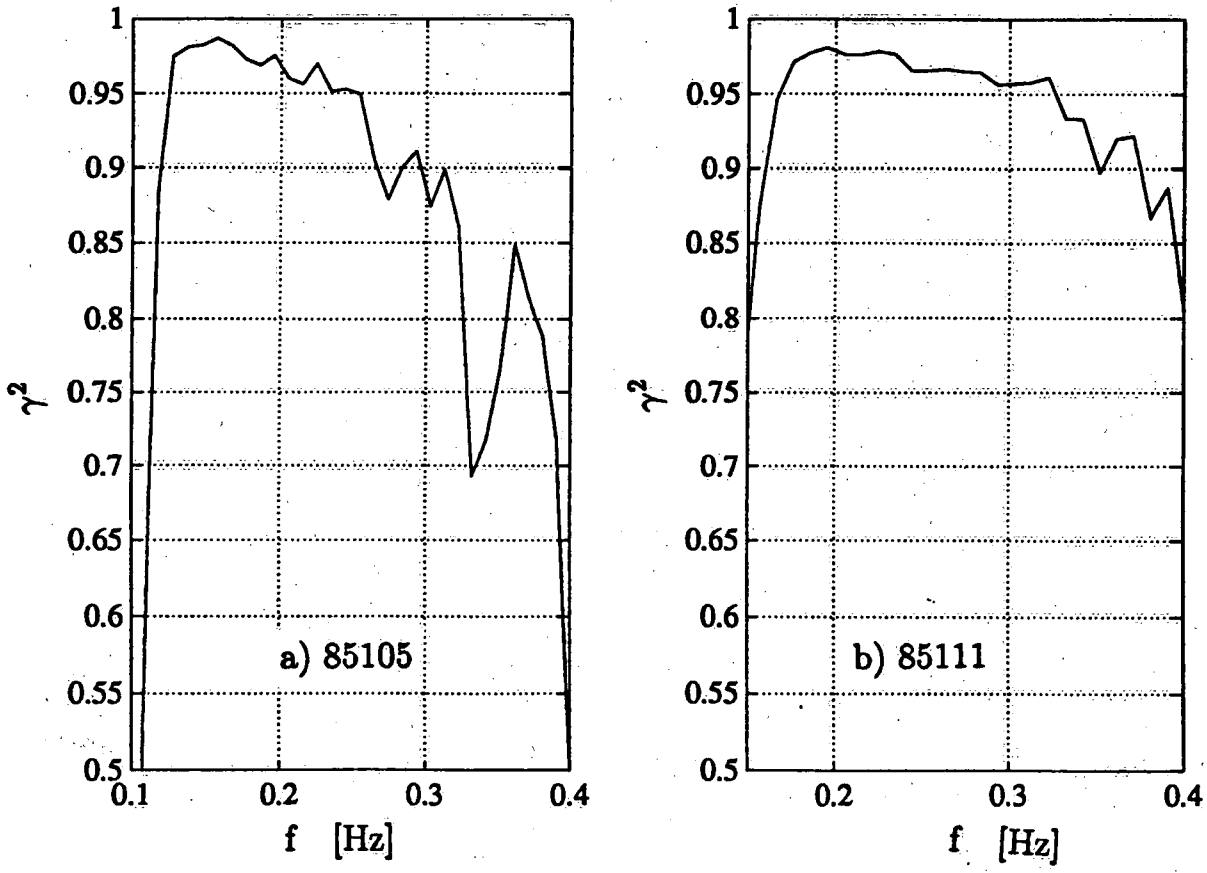

Figure 11: Coherence between horizontal and vertical velocities, γ^2.

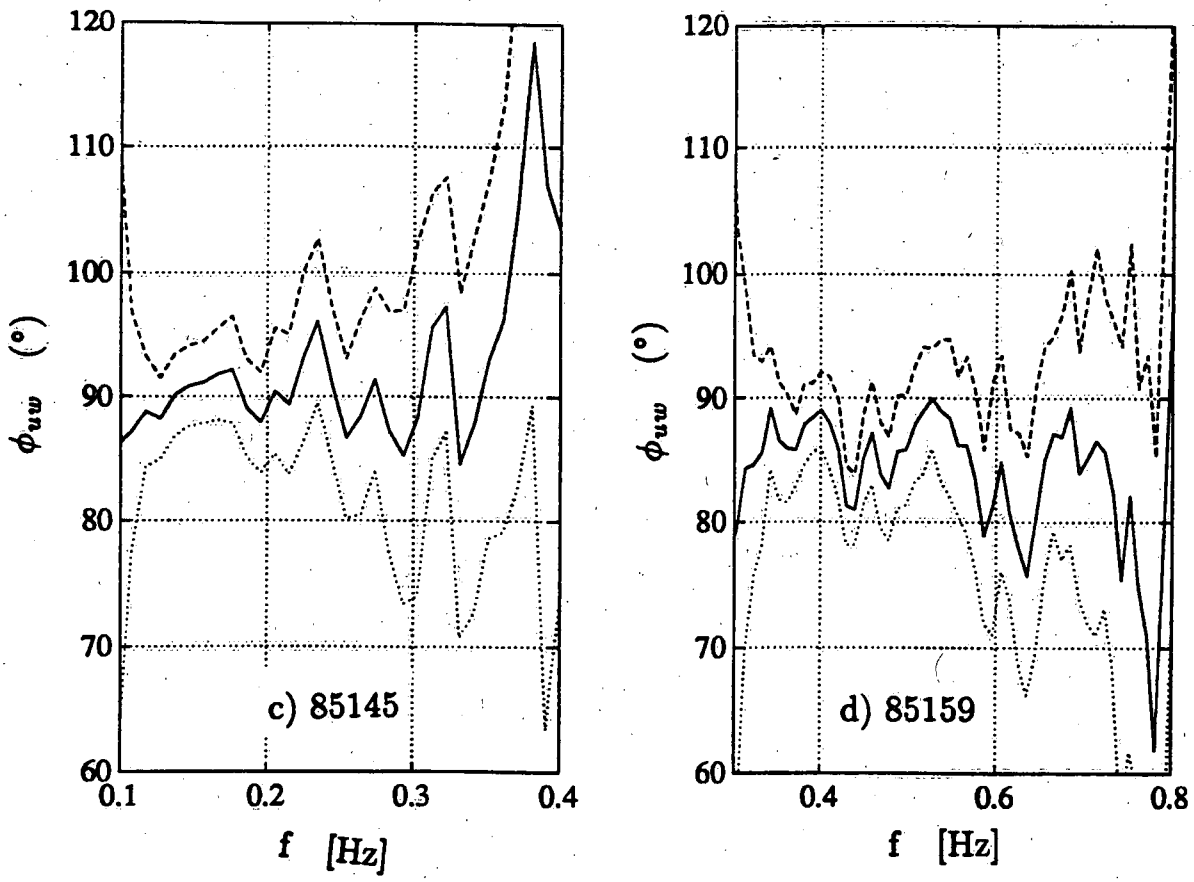

Figure 10: continued

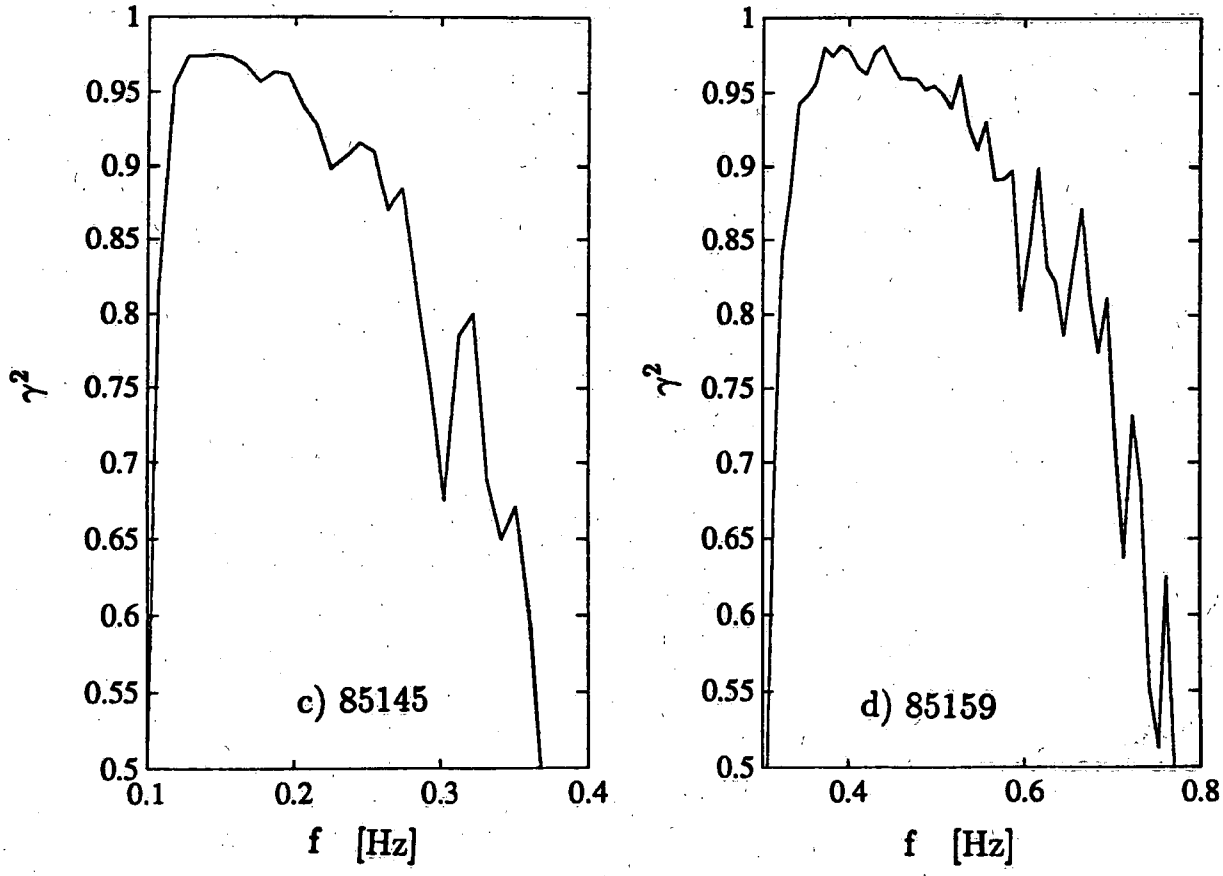

Figure 11 (continued)

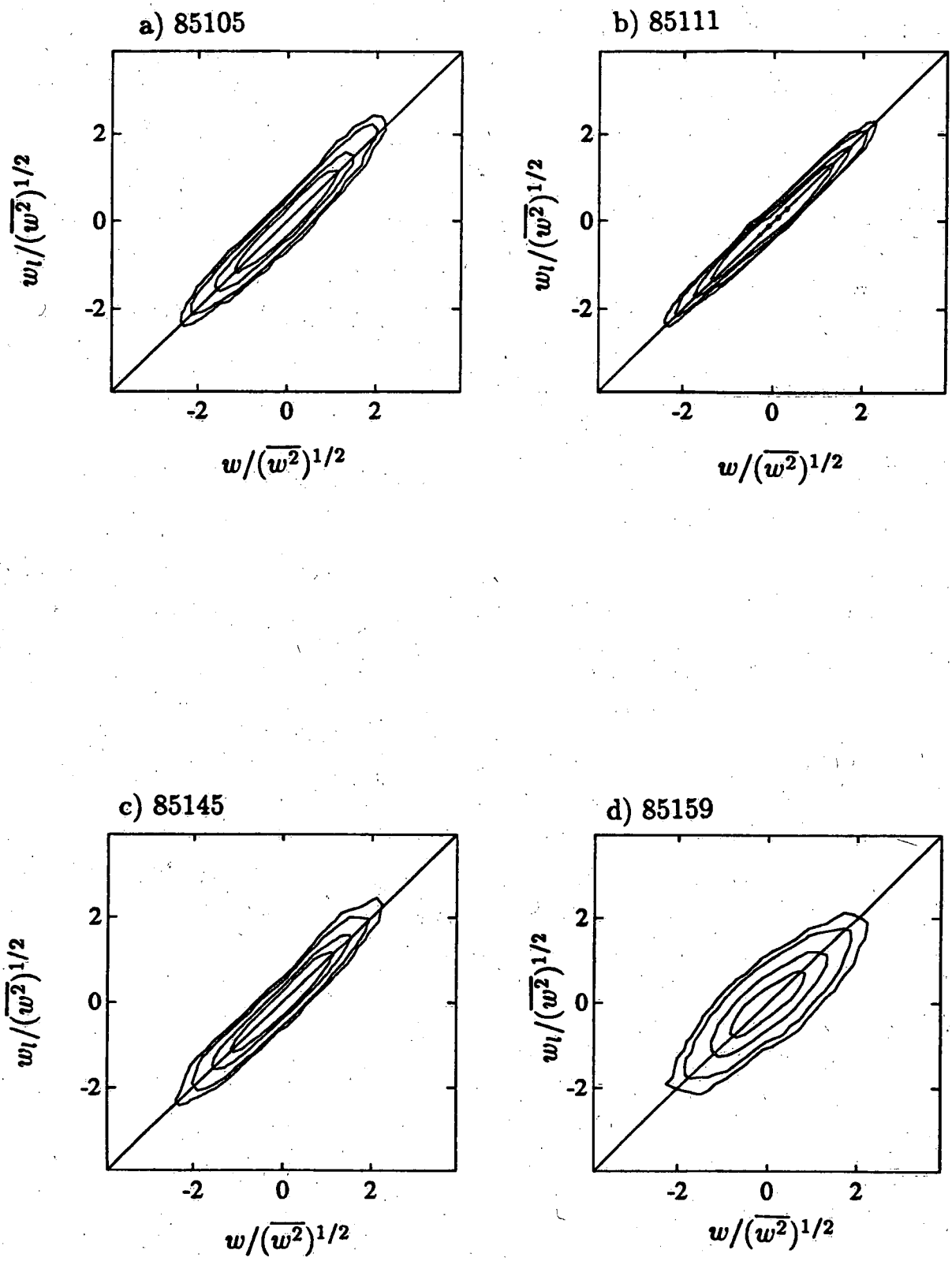

Figure 12: Joint frequency distributions of u and u_l, w and w_l.

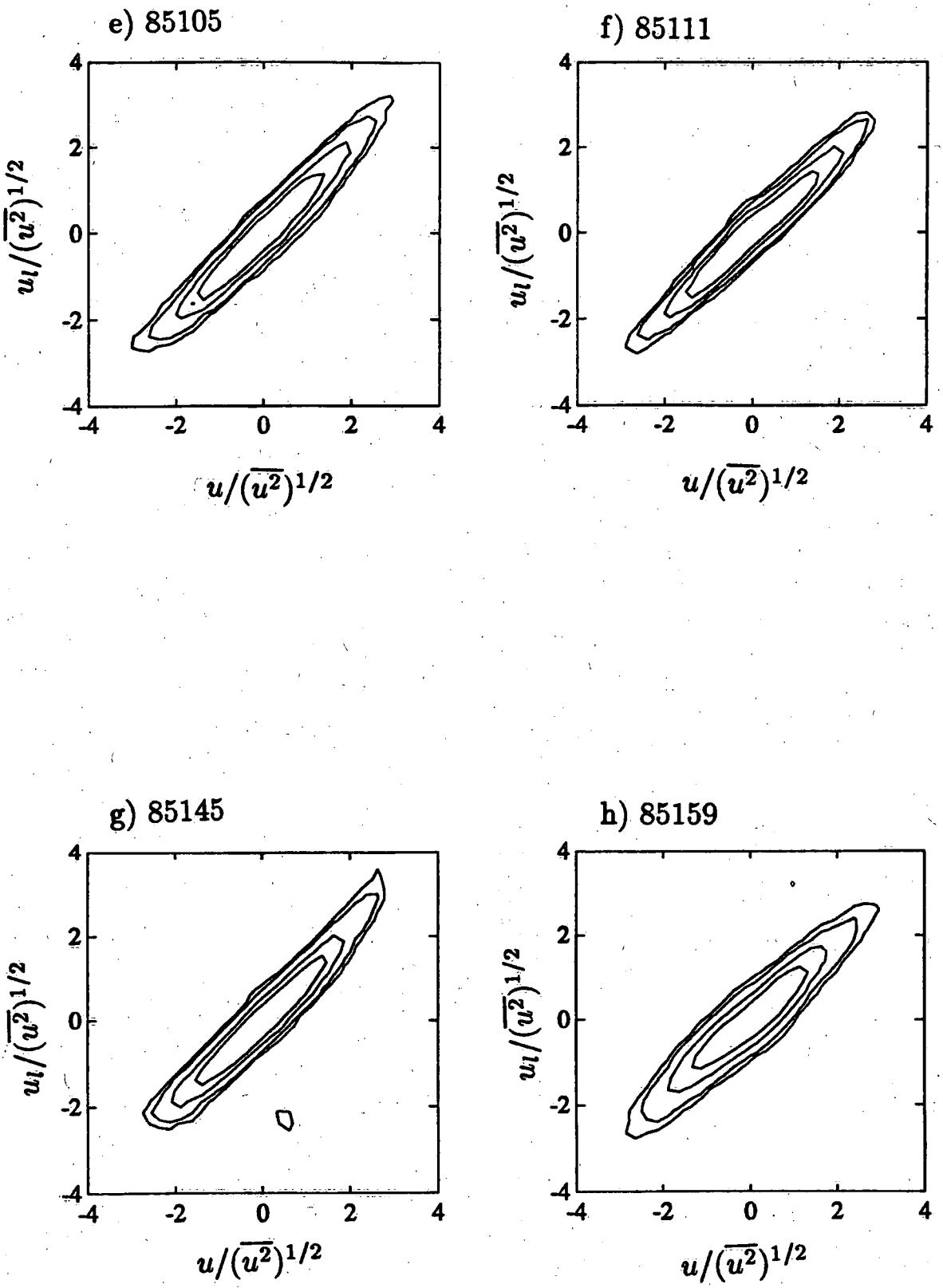

Figure 12 (cont'd) : Joint frequency distributions of u and u_l

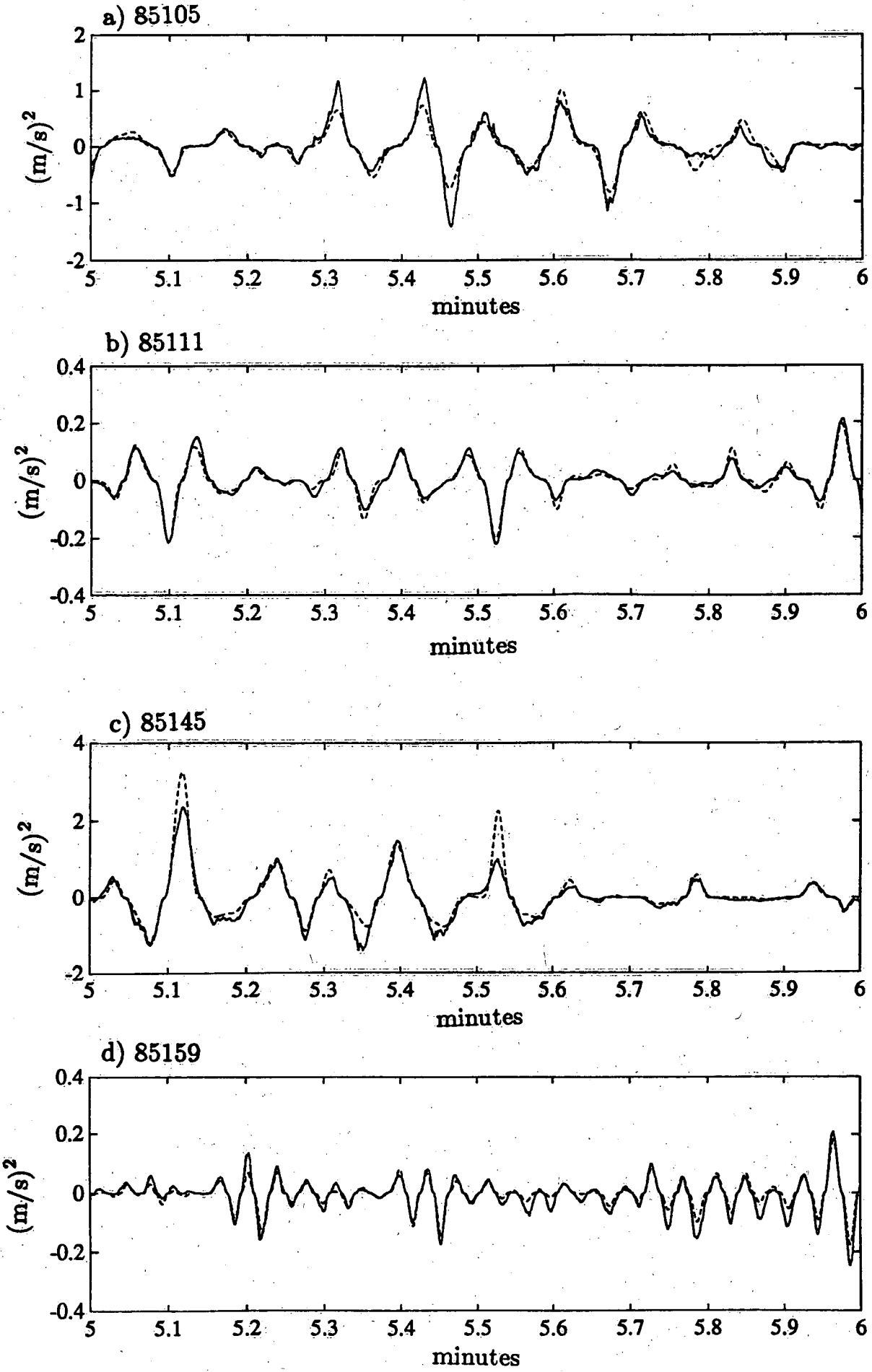

Figure 13: Time series of $u\,|u|$ (—) and $u_l\,|u_l|$ (- -).

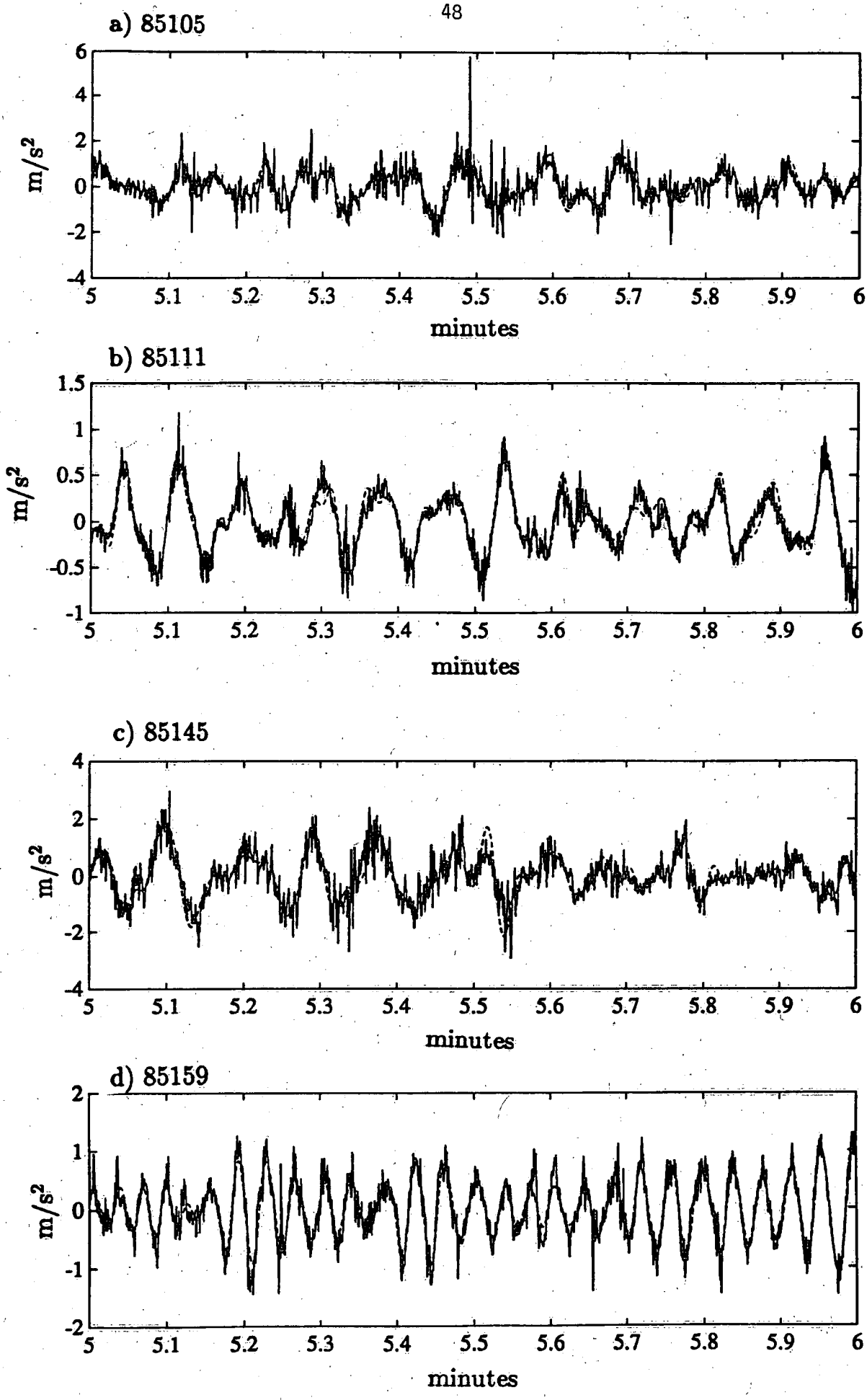

Figure 14: Time series of $\dot{u}$ (—) and $\dot{u}_l$ (- -)

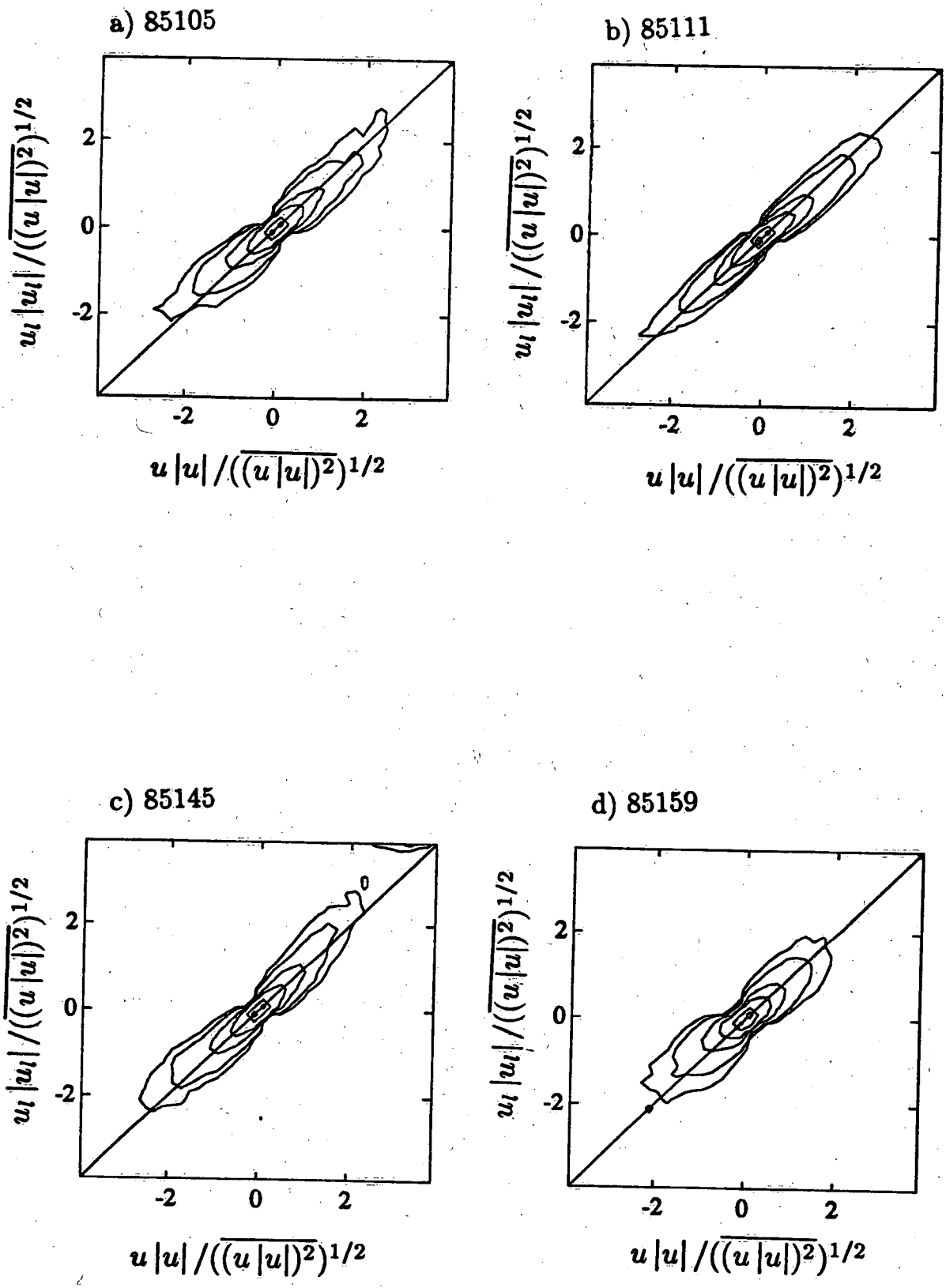

Figure 15: Joint frequency distributions of $u\,|u|$ and $u_l\,|u_l|$.

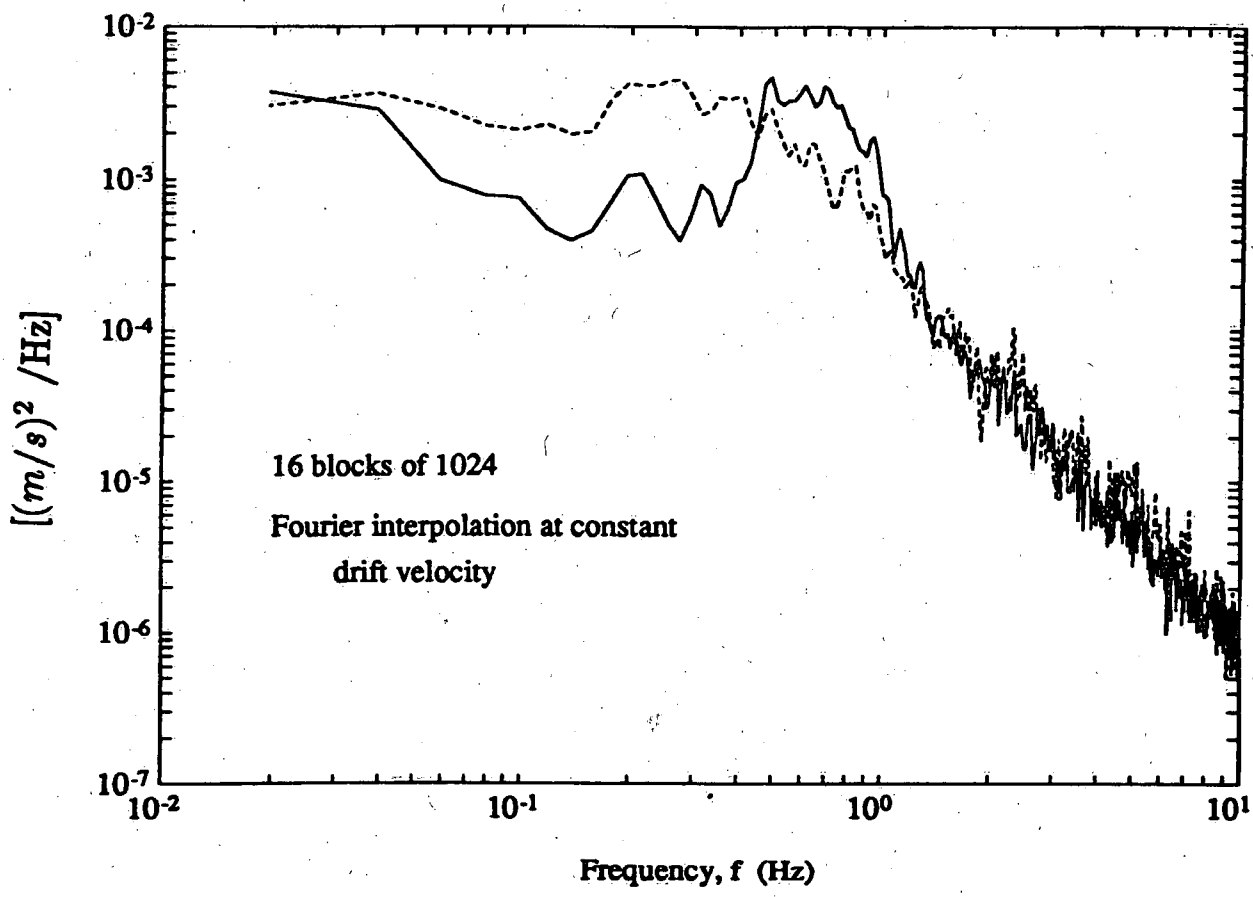

Figure 16: Spectra of turbulent component of vertical velocity, run 87091, with (—) and without (- -) Fourier interpolation. Turbulent component is obtained after removing wave-coherent component through filtering. (See Kitaigorodskii *et al.*, 1983).

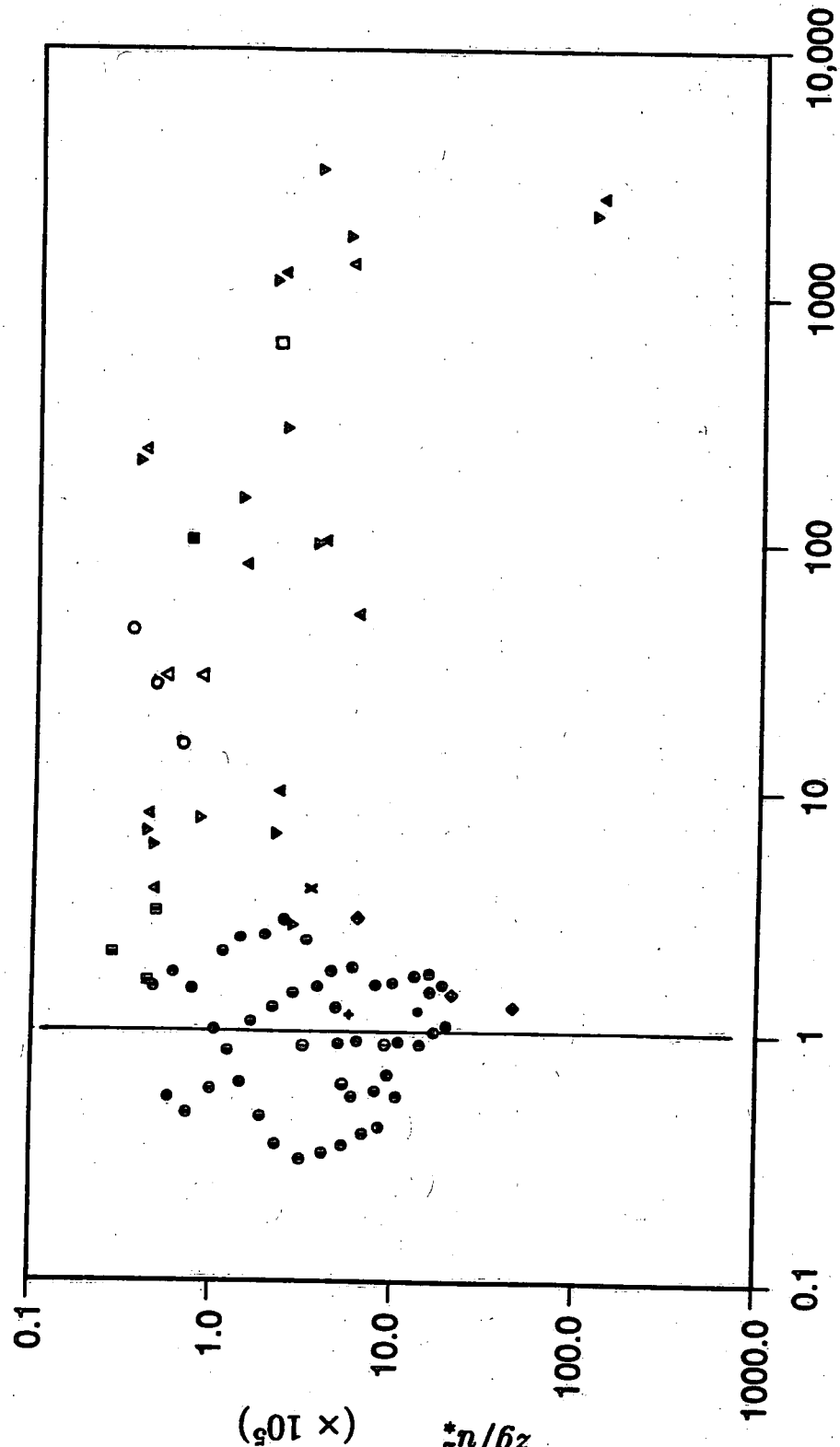

Figure 17: Dissipation in 'wall layer' coordinates $\epsilon\kappa z/u_*^3$ versus zg/u_*^2. The 'law of the wall' appears as the vertical line (—). For symbols, see Table 4.

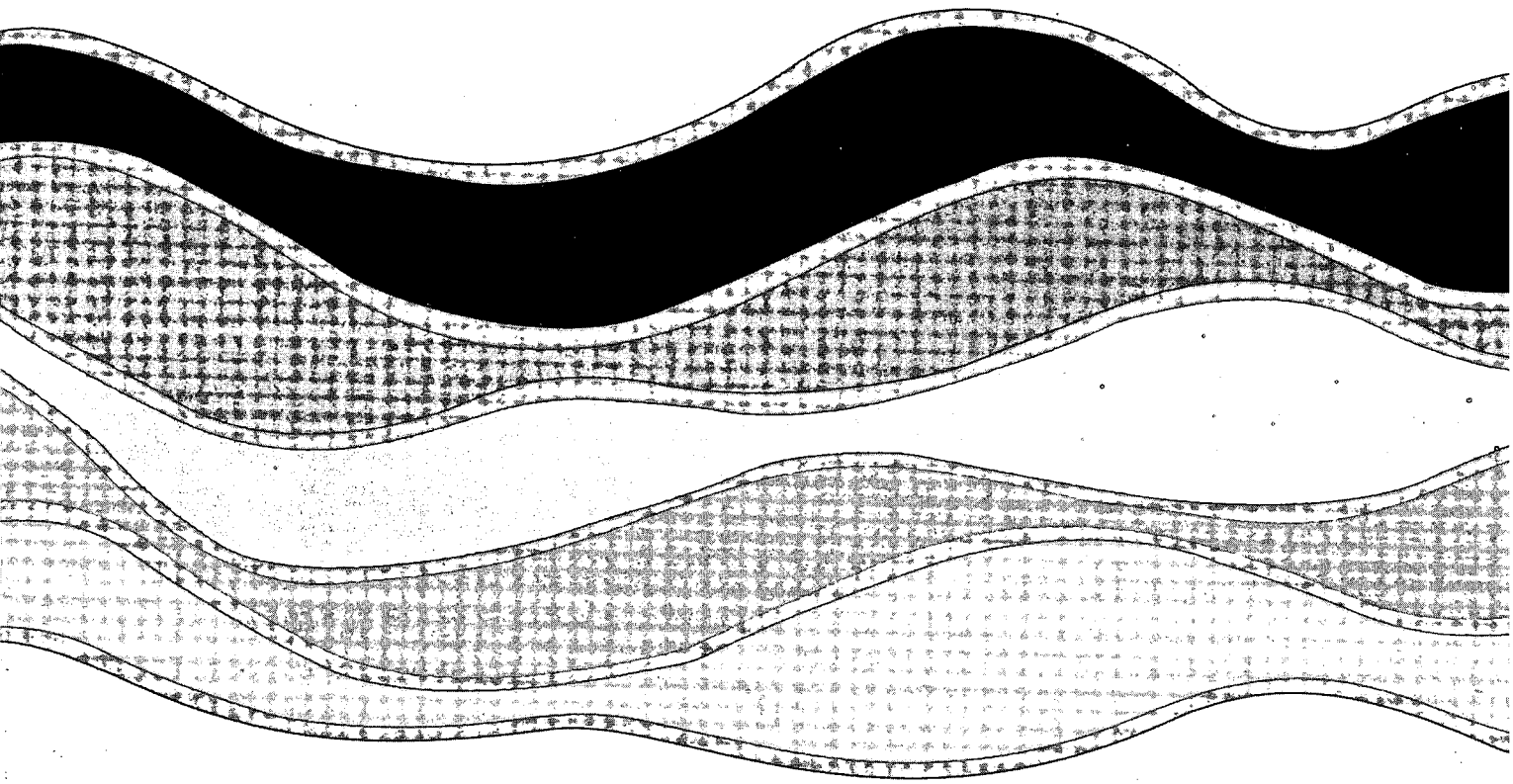

NATIONAL WATER RESEARCH INSTITUTE
P.O. BOX 5050, BURLINGTON, ONTARIO L7R 4A6

Environment Canada Environnement Canada

Canada

INSTITUT NATIONAL DE RECHERCHE SUR LES EAUX
C.P. 5050, BURLINGTON (ONTARIO) L7R 4A6